

Studies of spin relaxation and molecular dynamics in liquid crystals by two-dimensional Fourier transform electron spin resonance.

II. Perdeuterated-tempone in butoxy benzylidene octylaniline and dynamic cage effects

V. S. S. Sastry,^{a)} Antonino Polimeno,^{b)} Richard H. Crepeau, and Jack H. Freed
Baker Laboratory of Chemistry, Cornell University, Ithaca, New York 14853-1301

(Received 21 March 1996; accepted 24 May 1996)

Two-dimensional Fourier transform (2D-FT)-electron spin resonance (ESR) studies on the small globular spin probe perdeuterated tempone (PDT) in the liquid crystal solvent 4O,8 (butoxy benzylidene octylaniline) are reported. These experiments, over the temperature range of 95 °C to 24 °C, cover the isotropic (*I*), nematic (*N*), smectic *A* (*S_A*), smectic *B* (*S_B*), and crystal (*C*) phases. The 2D-ELDOR (two-dimensional electron–electron double resonance) spectra confirm the anomalously rapid reorientation of PDT, especially in the lower temperature phases. The model of a slowly relaxing local structure (SRLS) leads to generally very good non-linear least squares (NLLS) global fits to the sets of 2D-ELDOR spectra obtained at each temperature. These fits are significantly better than those achieved by the standard model of Brownian reorientation in a macroscopic orienting potential. The SRLS model is able to account for anomalies first observed in an earlier 2D-ELDOR study on PDT in a different liquid crystal in its smectic phases. Although it is instructional to extract the various spectral densities from the COSY (correlation spectroscopy) and 2D-ELDOR spectra, the use of NLLS global fitting to a full set of 2D-ELDOR spectra is shown to be more reliable and convenient for obtaining optimum model parameters, especially in view of possible (incipient) slow motional effects from the SRLS or dynamic cage. The cage potential is found to remain fairly constant at about $k_B T$ over the various phases (with only a small drop in the *S_B* phase), but its asymmetry increases with decreasing temperature *T*. This value is significantly larger than the weak macroscopic orienting potential which increases from 0.1 to $0.3k_B T$ with decreasing *T*. The cage relaxation rate, given by R^c is about $3 \times 10^7 \text{ s}^{-1}$ in the *I* phase, but increases to about 10^8 s^{-1} in the *S_A*, *S_B*, and *C* phases. The rotational diffusion tensor for PDT shows only a small *T*-independent asymmetry, and its mean rotational diffusion coefficient is of order 10^{10} s^{-1} , with however, a small increase in the *S_B* phase. These results are consistent with a model previously proposed for PDT in benzylidene liquid crystal solvents, that as *T* is reduced the PDT molecules are partially expelled from the hard core (dipolar) region of the liquid crystalline molecules toward the more flexible aliphatic chain region as a result of increased core packing from smectic layer formation, and it thus experiences a more fluid (for a given temperature) local cage structure. © 1996 American Institute of Physics. [S0021-9606(96)51333-4]

I. INTRODUCTION

In this paper we continue our studies of rotational relaxation by two-dimensional Fourier transform (2D-FT) electron spin resonance (ESR) methods. We study the relatively small nitroxide probe, perdeuterated-tempone (PDT) dissolved in the liquid crystal 4O,8, which was also used in the companion paper¹ (Part I). The PD-tempone probe has been used extensively as a solute in a wide range of liquid crystal solvents. Its rotational mobility has been utilized to probe the dynamic molecular structure of these solvents,^{2–5} a topic that has been reviewed recently.⁶ Its small size ($\sim 3.2 \text{ \AA}$ molecular radius) means that it is in the motional narrowing regime in most liquid crystalline phases, despite their increased viscosity.

In an early 2D-FT electron–electron double resonance (2D-ELDOR) study PD-Tempone was examined in the smectic *A* (*S_A*) phase of a mixed cyano-biphenyl liquid crystal solvent (S2) which extended over a substantial temperature range,⁴ and its anisotropic translational diffusion has since been examined in that phase as well.⁷ This study of translational diffusion showed that PD-Tempone exhibits effects that relate to its small size relative to the liquid crystal molecules and thus to the size of the smectic bilayers that form ($\sim 30 \text{ \AA}$). (Smectic layers in 4O,8 are about this thickness judging from the value of 26.8 \AA measured for 4O,7.⁸) That is, diffusion of PDT within the smectic layers (given by transverse diffusion coefficient, D_{\perp}) is always greater than traversing them (given by longitudinal diffusion coefficient, D_{\parallel}), such that $D_{\perp}/D_{\parallel} > 1$. The standard model, due to Volino and Dianoux⁹ and Moro *et al.*,^{10,11} is that the longitudinal diffusion of a small globular probe over times long compared to the time of traversing a single smectic layer, can be described as a random jump over the barrier of the hard-

^{a)}On leave of absence from School of Physics, University of Hyderabad, Hyderabad 500 134, India.

^{b)}On leave of absence from Department of Physical Chemistry, University of Padova, Via Loredan 2, 35131 Padova, Italy.

core region of the smectic layer in addition to the normal diffusive factors that also affect D_{\perp} . Thus D_{\parallel} experiences an extra contribution to its activation energy, which Moscicki *et al.*⁷ interpret in terms of a model of the free volume redistribution within the smectic liquid. In these models, the potential energy of the probe depends on both its orientation and its location within the smectic layer, so there is translational–rotational coupling. That is, the PDT will experience a greater orienting potential when it is near the hard core region of the smectic layers, and a reduced potential when it is in the aliphatic chain region. Also, the probe will have a preference for where it resides within the layer. In addition, extensive evidence from past cw-ESR results is consistent with a model in which PDT molecules are partially expelled from the hard core (dipolar) region of the liquid crystalline molecules toward the more flexible hydrocarbon end chains as a result of the packing of the smectic layers.^{3,6} This partial expulsion is clearly enhanced by the smectic layer formation as the temperature is reduced. It was suggested that, concomitant with this partial expulsion, the PDT increasingly experiences a slowly relaxing local structure (SRLS) in a cavity-like location.^{3,6} Given the limited information content of fast motional cw-ESR spectra in macroscopically aligned phases [i.e., 3 hyperfine (hf) lines each with a linewidth and a resonant magnetic field position], as well as the fact that sample mosaicity and proton super hfs can obscure the homogeneous contribution to the linewidth, only inferences of a preliminary nature could be made about the appropriateness of the SRLS model. Additionally, the theory available at that time was not precisely formulated for ordered phases.³

In the 2D-ELDOR study by Gorcester *et al.* (referred to as GRF) on PDT in the S_A phase of S2, an attempt was made to fit the 2D-ELDOR cross-peaks to the model of translational–rotational coupling outlined in the previous paragraph.⁴ It appeared to be successful in dealing with the orientation dependence of the cross-peak intensities, from which W_n , the nuclear spin-flip rate, is obtained. But it could not at the same time successfully predict the rather large homogeneous T_2^{-1} 's measured and their insensitivity to orientation of the smectic layers relative to the applied dc magnetic field. It was suggested⁴ that there is an additional contribution to T_2^{-1} arising from cooperative aliphatic chain fluctuations, i.e., the basic SRLS mechanism (also outlined in the previous paragraph).

In the present study on PDT in 4O,8 solvent by modern 2D-ELDOR methods,^{12,13} we can take advantage of improved instrumental capabilities which have led to better spectral coverage, shorter spectrometer dead times, and greatly enhanced signal averaging capabilities.^{14,15} We also have, in 4O,8, a liquid crystal that exhibits several ordered phases, each with a substantial temperature range. Furthermore 4O,8, unlike S2, exhibits a monolayer smectic phase.⁶

Our principal objectives in the present study were to see if we could achieve a consistent interpretation of all the features of the 2D-ELDOR, viz. auto- and cross-peak intensities and their homogeneous widths, in terms of the new version for SRLS developed by Polimeno and Freed¹⁶ and adapted

for 2D-FT-ESR in Paper I, and also to see how the results for the SRLS model depended on the different phases. Given that we wished to fit all aspects of the 2D-ELDOR experiments, we emphasize in this work the global fitting procedure based on nonlinear least squares (NLLS) methods utilized in Paper I. In this procedure one forgoes the decomposition of the fast-motional spin-relaxation into the various spectral densities⁶ in favor of the simultaneous fitting of the sets of 2D-ELDOR spectra (as a function of mixing time, T_m) to the fundamental molecular ordering and dynamic parameters.^{17,18} Nevertheless, we do also consider in some detail salient features of the key spectral densities one obtains from these experiments.

Given the significant differences between PDT, which is sensitive to precise location in a smectic layer, and the larger, rigid CSL probe studied in Paper I, which does not show roto-translational coupling effects, it is of additional interest to compare the respective features of the SRLS model that emerge from these studies. We can ask the question of how similar is the nature of the dynamic cage which influences the reorientational motion of these two probes in the same liquid crystalline solvent.

We show in Fig. 1 typical 2D-ELDOR spectra of PDT in 4O,8 in the different phases (I , N , S_A , S_B , and C) at a fixed mixing time. We clearly see very sharp auto- and cross-peaks for all the phases that signal the motionally narrowed regime. These are distinctly different from the very broad CSL spectra (cf. Paper I), as expected. In all phases the cross-peaks are very weak, characteristic of very fast rotational reorientation. It makes clear that there is no appreciable slowing down of the motion as the temperature is lowered into the different liquid crystalline phases, an unusual behavior, which we examine in the context of the SRLS model.

In Sec. II we present the experimental details. Our results are presented in Sec. III, with a discussion in Sec. IV and conclusions in Sec. V.

II. EXPERIMENTAL DETAILS

The liquid crystal (4O,8) was prepared earlier in this laboratory, and the transition temperatures were confirmed by differential scanning calorimetry (DSC) measurements as:



The nitroxide free radical 2,2,6,6-tetramethyl-4-piperidone-*N*-oxyl-d16 (PD-Tempone = PDT) was synthesized by E. Igner and solutions of this radical in 4O,8 at a concentration of about 1×10^{-3} M were prepared by mixing them very well for a prolonged period just above the clearing temperature. Samples were prepared in 2-mm-o.d. glass tubes after deoxygenating them by standard procedures and sealing them under vacuum.

2D-ESR experiments [correlation spectroscopy (COSY) and ELDOR] were carried out on a home-built Fourier transform (FT)-ESR^{12–14} spectrometer as a function of temperature covering all the phases. In these measurements the sample was aligned and the director was kept parallel to the

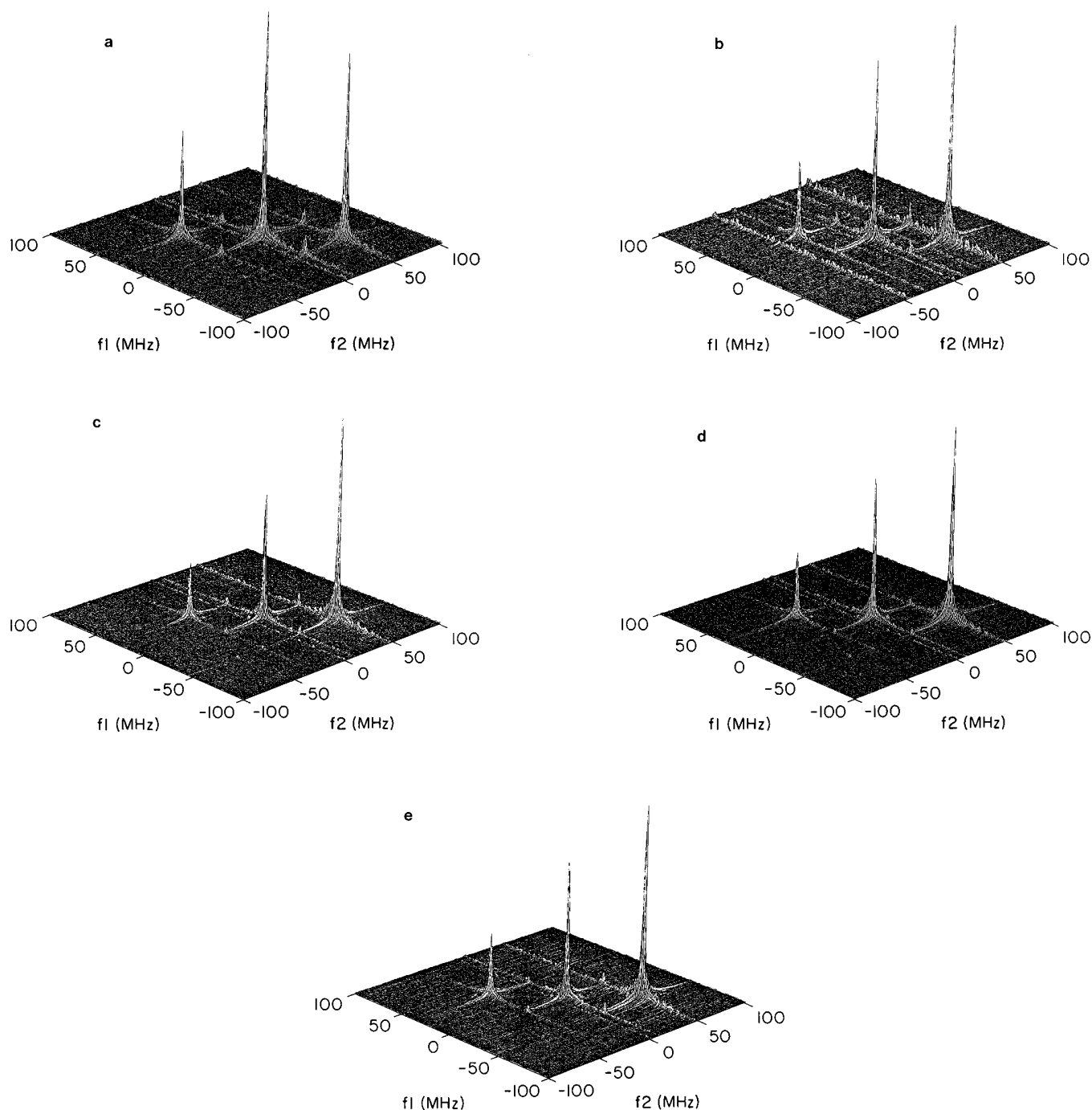


FIG. 1. ELDOR Magnitude spectra of PDT in 4O.8 in different phases at a fixed mixing time of 600 ns, (a) 90 °C—isotropic; (b) 72 °C—nematic; (c) 57 °C—smectic A; (d) 39 °C—smectic B; (e) 24 °C—crystal. Note the weak cross-peaks.

magnetic field. Additional COSY measurements were made in the S_A and S_B phases, as a function of the orientation of the director with respect to the magnetic field. The width of a $\pi/2$ pulse was typically about 5 ns which provides a nearly uniform spectral rotation into the rotating x - y plane over at least a ± 75 MHz bandwidth.¹³⁻¹⁵ The free induction decay (FID) after the last pulse was sampled every 5 ns corresponding to the time resolution in the t_2 direction, providing 256 data points. The separation between the first two pulses, t_1 , was stepped in 128 steps of 5 ns each. The spectrometer dead

time, τ_d , was 60 ns, while the minimum separation between pulses was 50 ns. A 32 (8) step dual quadrature phase cycling sequence for 2D-ELDOR (COSY) provided the complex signal with respect to t_1 and t_2 , and it provided for subtraction of all unwanted signals.¹²⁻¹⁵ Each step in the phase cycling sequence was an average of 500 repetitions obtained at a 10 kHz rate.

The sample temperature was regulated using a gas flow type cryostat with a commercial temperature controller (Bruker model ER 4111 VT) to an accuracy of about ± 1 K.

The magnetic field was stabilized using a standard field-frequency lock arrangement (Varian Fieldial, Mark II), leading to a typical field stability better than ± 10 mG (or about 3 parts in 10^6) during a 20 minute data collection. The microwave frequency was stabilized to an accuracy of about ± 1 kHz (or about 1 part in 10^7) using a Microwave Systems Inc. metal-oxide semiconductor (MOS) lock box. Rotation of the static magnetic field with respect to the director is effected by mounting the sample on a suitable goniometer.

The COSY spectra of PDT were recorded, using a $\pi/2-t_1-\pi/2-t_2$ sequence, and the dual quadrature data were then subjected to a shearing transformation to provide equivalent electron spin-echo results for purposes of computing homogeneous linewidths (see the discussion below). In the S_A and S_B phases these measurements were carried out as a function of the orientation of the director with respect to the static magnetic field at two temperatures in each phase. The 2D-ELDOR measurements were performed with a $\pi/2-t_1-\pi/2-T_m-\pi/2-t_2$ sequence for different mixing times (T_m). Typically, spectra were recorded for at least six mixing times ranging from 300 or 400 ns to 1400 ns, the signal to noise ratio being the limiting factor for stepping out T_m further. The average time to record a data set for each mixing time was about 20 minutes.

Instrumental artifacts arising out of the interaction of the microwave pulses for values of t_1 less than 200 ns were corrected for by deconvoluting the data with an instrumental response function.¹⁵ This is done by obtaining, under identical experimental conditions, 2D spectra on a reference sample with sharp and well-defined lines. In particular, we used a solution of PDT in toluene. The idea is to use the signal of the reference in the error free time domain (i.e., $t_1 > 200$ ns) and linear prediction¹² to correct earlier time domain behavior (i.e., $t_1 < 200$) which has been corrupted in the experiment by instrumental artifacts. The filter function, $F(t_1)$, generated by comparing this prediction with the actual experimental data from the reference, accounts for the extra phase and amplitude modulations induced by such pulse interference. The actual signals from the liquid crystal samples were then corrected by multiplication by $F(t_1)$, leading to substantially improved experimental 2D results.

Another correction was found necessary for larger intervals of t_1 , particularly in the present experiments where $t_{1,\max} = 690$ ns. Large spikes occasionally appeared for larger t_1 values, presumably due to a noise fluctuation, which yielded incomplete cancellation of the FID signal after the third pulse that arises from the magnetization that had recovered from the previous pulses. This spiky noise is observed only for fairly long t_1 values (typically greater than 500–600 ns) where the ELDOR signal has already decayed appreciably. However, the signal is clean and significantly noise free for the early t_1 values. Thus, this region of data was used to linearly predict the time domain complex information for longer t_1 values, thereby providing an approximation to the signal in that region. This predicted (dual quadrature) signal was then compared with the experiment, and only those experimental points which fell within a predetermined range of the corresponding predicted values were retained. The ex-

perimental points falling outside this range were replaced by an interpolation between the neighboring points. In the present case, all experimental points which deviated from the predicted values by more than five times the root mean square (rms) deviation were replaced by the above procedure (see Ref. 4 for details).

By means of linear prediction methods it was possible to extract the pure absorption-absorption spectra by procedures discussed elsewhere.¹² The linearly predicted forms of the filtered data were then used to extract spectral densities. However, when comparing spectral simulations to experimental data, we utilized the original but filtered and doubly Fourier transformed spectra displayed as magnitude spectra for convenience. We used the S_{c-} combination, which corresponds to the echo-like coherence pathway.^{17,19} There was almost no difference between the S_{c-} and S_{c+} (or FID-like pathway) combinations in all cases. The spectra are displayed for the frequency range of -100 MHz to 100 MHz along both f_1 and f_2 . For comparison of simulated and experimental spectra it was found necessary to first extend the t_1 and t_2 ranges by a factor of 2 by zero filling prior to the double fast Fourier transform (FFT) in order to provide the needed frequency resolution in f_1 and f_2 . For purposes of comparing the experiments with simulations, corrections were made for the spectrometer coverage obtained from a set of single pulse FID experiments measured over the range of magnetic field values covering the spectral bandwidth.¹⁵ Typical 2D ELDOR magnitude FT spectra at a representative temperature in each phase are shown in Fig 1, for a fixed mixing time of $T_m = 600$ ns.

The magnetic parameters of PDT in 4O,8 have been determined by Lin and Freed,³ who found that the hf tensor changes slightly with phase. We used their values, which are: $(A_{xx}, A_{yy}, A_{zz}) = (5.58, 4.99, 33.5G)$ in the I phase; $(5.56, 4.97, 33.4G)$ in the N phase; $(5.54, 4.95, 33.3G)$ in the S_A phase; and $(5.51, 4.92, 33.1G)$ in the S_B phase; $(g_{xx}, g_{yy}, g_{zz}) = (2.0099; 2.0062; 2.00215)$. The phase dependence of the hf tensor for PDT is interpreted in terms of the partial expulsion of PDT from the hard core region of the liquid crystal molecules, noted in Sec. I. Following common practice, we shall refer to the principal axes of these magnetic tensors as (x''', y''', z''') and the principal axes of diffusion taken as coincident with the principal axes of alignment for the PDT molecule as (x', y', z') .^{3,6,18,20} The x''' -axis is along the N–O bond, and the z''' -axis is along the nitrogen p - π orbital, with the y''' -axis perpendicular to both. Following the previous studies,^{3,6} we have taken the y''' -axis to be the principal axis of alignment such that $y''' \parallel z'$, and also $x''' \parallel x'$ with $z''' \parallel y'$.

III. RESULTS

A. The orientational order parameters

Measurements of the effective hyperfine splitting, $\langle a \rangle$ and of the effective g -factor, $\langle g \rangle$ in oriented media have in the past been used extensively to obtain the macroscopic order parameters $\langle \mathcal{P}_{00}^2 \rangle$ and $\langle \mathcal{P}_{02}^2 + \mathcal{P}_{-2}^2 \rangle$ for the spin-probe from motionally narrowed spectra.⁶ We find that the use of

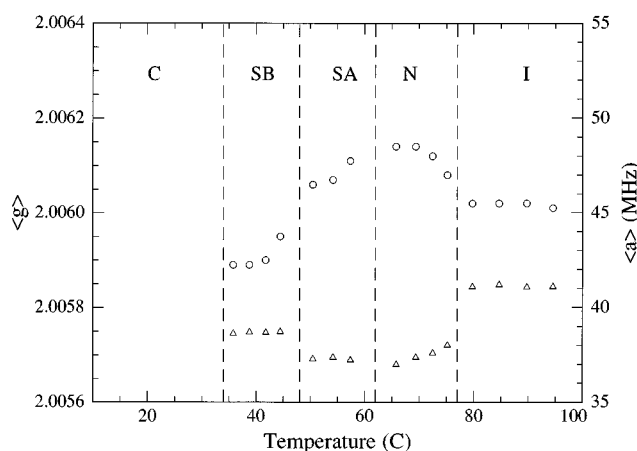


FIG. 2. $\langle g \rangle$ (open circles) and $\langle a \rangle$ (open triangles) versus temperature. From single pulse FID measurements.

modern FT methods improves the accuracy of these measurements over conventional cw-ESR methods. This arises because the FT spectra have the dc magnetic field, B_0 , maintained at a constant value, whereas in cw-ESR, B_0 is swept and one must calibrate this sweep. Also, the microwave frequency is kept locked to a constant value. Thus, the frequency axis of the FT spectrum is known to high accuracy.¹² The only calibration required is the magnetic field offset between that at the sample location and that at the gaussmeter probe. Single pulse FIDs were collected at each temperature, with the director aligned with the magnetic field. They were Fourier transformed to provide the magnitude ESR spectrum, and the locations of the three spectral lines on the frequency axis were determined by a simple curve fitting procedure. Using the known value of $\langle g \rangle = g_s$ of PDT in the isotropic liquid phase of 4O,8,³ the FT spectrum for this phase was used to calibrate the magnetic field offset. The positions of the three spectral lines in the other phases were then used to obtain the variation of $\langle g \rangle$ and $\langle a \rangle$ with temperature (Fig. 2). Such single pulse FID spectra were also collected as a function of the angle between the director and the field in the S_A and S_B phases, enabling confirmation of the isotropic part of the hyperfine interaction in these phases (the isotropic value, g_s , does not exhibit any observable change with phase). Then, using standard procedures,⁶ the hyperfine tensor, and g -tensor of PDT, the macroscopic order parameters $S_0^2 = \langle \mathcal{D}_{0,0}^2(\Omega^o) \rangle$ and $S_2^2 = \langle \mathcal{D}_{0,2}^2(\Omega^o) + \mathcal{D}_{0,2}^2(\Omega^o) \rangle$ (cf. Eq. 43 of Paper I) were determined vs temperature (Fig. 3). These results are, of course, quite similar to the results of Lin and Freed.³ However, they show that $\langle g \rangle$ and $\langle a \rangle$ have no substantial discontinuity at the $N-S_A$ transition as expected for a second order transition.⁵ The results of Lin and Freed are erroneous in this respect for $\langle g \rangle$ as previously pointed out,²¹ and this led to inaccuracies in S_0^2 and S_2^2 .

B. The homogeneous T_2 's

The choice of the S_c - combination in the COSY experiments permits a "shearing transformation" to be performed

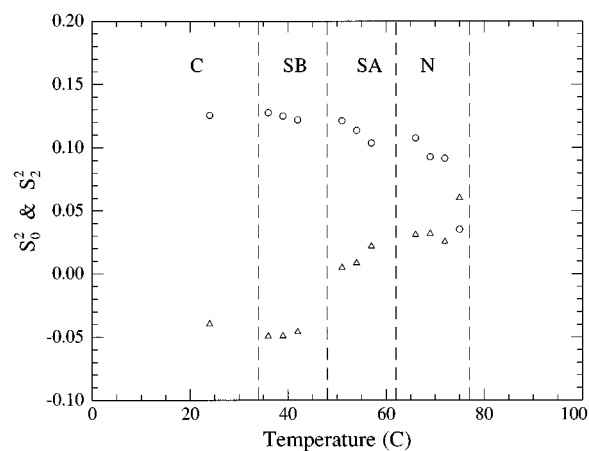


FIG. 3. Mean field order parameters: $S_0^2 = \langle \mathcal{D}_{0,0}^2 \rangle$ (open circles), and $S_2^2 = \langle \mathcal{D}_{0,2}^2 + \mathcal{D}_{0,2}^2 \rangle$ (open triangles), versus temperature. From single pulse FID measurements.

on the time domain data by using the data for which $t_2 > t_1$, and then letting $t_2 \leftarrow t_1 + t_2$.^{17,22} This leads to a SECSY-based experimental result, even though the actual experiment was performed by simply collecting the FIDs after the sampling pulse. This technique is particularly useful in that it permits the determination of the homogeneous linewidths (T_2^{-1}) of the three spectral lines. The procedure adopted for the present purpose involved application of the shearing transformation to the time domain data, followed by Fourier transformation along the t_2 direction, resulting in a spectrum in t_1 and f_2 comprising magnitude ESR spectra (along f_2) stacked together in the t_1 direction. Given the well resolved spectra in the motionally narrowed regime, it was simple to find the decay constants of the three hf lines along t_1 , yielding the homogeneous linewidths of the three spectral lines. The COSY experiments, with the director parallel to the field, thus provided the variation of T_2 's of the different hyperfine lines as a function of temperature.

The T_2 's of the different hyperfine lines have the well known dependence on the z component of the nuclear spin M_I , given in the motional narrowing region by:⁶

$$T_2(M_I)^{-1} = A + BM_I + CM_I^2, \quad (2)$$

$$A - A' = 2J_1^{AA}(\omega_a) + \frac{2}{3}J_0^{AA}(\omega_e) + 4J_2^{AA}(\omega_e) + \frac{8}{3}J_0^{gg}(0) + 2J_1^{gg}(\omega_e), \quad (3)$$

$$B = \frac{16}{3}J_0^{Ag}(0) + 4J_1^{Ag}(\omega_e), \quad (4)$$

$$C = \frac{8}{3}J_0^{AA}(0) - J_1^{AA}(\omega_a) + 2J_1^{AA}(\omega_e) - \frac{1}{3}J_0^{AA}(\omega_e) - 2J_2^{AA}(\omega_e), \quad (5)$$

where A and g indicate respectively electron-nuclear dipolar and g -tensor interactions of the electron. A' represents line-broadening independent of the rotational modulation of these interactions (e.g., Heisenberg spin exchange and spin-rotational relaxation),²⁰ and it will be represented as $A' \equiv T_{2e}^{-1}$ below.

TABLE I. Zero frequency spectral densities for PDT in 4O,8.

| Phase | T (°C) | $-J_0^{Ag}(0) \times 10^6$ (s $^{-1}$) | $+J_0^{AA}(0) \times 10^6$ (s $^{-1}$) | $+J_1^{AA}(\omega_a) \times 10^6$ (s $^{-1}$) |
|----------------------|----------|---|---|--|
| <i>I</i> | 90.6 | 0.042 ± 0.003 | 0.168 ± 0.013 | 0.157 ± 0.006 |
| <i>I</i> | 85.2 | 0.052 ± 0.003 | 0.193 ± 0.015 | 0.190 ± 0.007 |
| <i>I</i> | 80.6 | 0.065 ± 0.003 | 0.168 ± 0.011 | 0.218 ± 0.007 |
| <i>N</i> | 73.5 | 0.061 ± 0.003 | 0.283 ± 0.015 | 0.251 ± 0.009 |
| <i>N</i> | 71.0 | 0.057 ± 0.003 | 0.235 ± 0.015 | 0.237 ± 0.007 |
| <i>N</i> | 68.4 | 0.074 ± 0.003 | 0.150 ± 0.014 | 0.188 ± 0.009 |
| <i>N</i> | 65.6 | 0.068 ± 0.005 | 0.234 ± 0.022 | 0.180 ± 0.005 |
| <i>S_A</i> | 58.6 | 0.099 ± 0.005 | 0.283 ± 0.022 | 0.162 ± 0.005 |
| <i>S_A</i> | 55.9 | 0.116 ± 0.005 | 0.302 ± 0.022 | 0.151 ± 0.004 |
| <i>S_A</i> | 53.3 | 0.124 ± 0.004 | 0.330 ± 0.022 | 0.139 ± 0.003 |
| <i>S_A</i> | 50.5 | 0.136 ± 0.008 | 0.366 ± 0.028 | 0.149 ± 0.005 |
| <i>S_B</i> | 44.4 | 0.046 ± 0.004 | 0.267 ± 0.016 | 0.041 ± 0.003 |
| <i>S_B</i> | 41.5 | 0.053 ± 0.004 | 0.269 ± 0.017 | 0.067 ± 0.003 |
| <i>S_B</i> | 38.8 | 0.054 ± 0.005 | 0.233 ± 0.022 | 0.075 ± 0.002 |
| <i>S_B</i> | 36.0 | 0.072 ± 0.005 | 0.267 ± 0.020 | 0.072 ± 0.003 |
| <i>C</i> | 29.0 | 0.112 ± 0.007 | 0.265 ± 0.026 | 0.090 ± 0.003 |
| <i>C</i> | 23.6 | 0.092 ± 0.009 | 0.383 ± 0.032 | 0.103 ± 0.003 |

For liquid crystal solvents with their substantial viscosity, non-secular terms are usually found to be unimportant (i.e., $J_M^{\mu\nu}(\omega_e) \ll J_M^{\mu\nu}(0), J_M^{\mu\nu}(\omega_a)$). Thus, we shall adopt the procedure of GRF of ignoring the non-secular terms and justifying this neglect *a posteriori*. Thus we have the remaining spectral densities $J_0^{Ag}(0)$, $J_0^{AA}(0)$, $J_1^{AA}(\omega_a)$, and $J_0^{gg}(0)$, which may be written in terms of observables:

$$J_0^{Ag}(0) = \frac{3}{16}B, \quad (6)$$

$$J_0^{AA}(0) = \frac{3}{8}[C + 2W_n], \quad (7)$$

$$J_1^{AA}(\omega_a) = 2W_n, \quad (8)$$

$$T_{2,e}^{-1} \equiv A' = A - 2J_1^{AA}(\omega_a) - \frac{8}{3}J_0^{gg}(0). \quad (9)$$

The nuclear spin-flip rate $2W_n$ may be obtained from the 2D-ELDOR cross-peak intensities as described below. Thus we can obtain $J_0^{Ag}(0)$, $J_0^{AA}(0)$, and $J_1^{AA}(\omega_a)$, but $J_0^{gg}(0)$ cannot be obtained from A unless $T_{2,e}^{-1}$ is known or inferred. We present in Table I the values of $J_0^{Ag}(0)$, $J_0^{AA}(0)$, and $J_1^{AA}(\omega_a)$ obtained in this manner. $J_0^{Ag}(0)$ and $J_0^{AA}(0)$ are also plotted vs T in Fig. 4(a) and they are fit to an Arrhenius plot for the S_A phase in Fig. 4(b). One sees that $J_1^{AA}(\omega_a) \approx J_0^{AA}(0)$ in the *I* phase as one expects for motional narrowing and an isotropic phase.⁶ However, in the smectic phases $J_1^{AA}(\omega_a) < J_0^{AA}(0)$, a result consistent with the previous observations for S2 solvent.⁴

The additional studies in both smectic phases, performed as a function of angle of the director with respect to the magnetic field, yielded the angular variation of the $T_2(M_I)^{-1}$. It was possible to decompose the spectral densities obtained in the angular variation studies by using the

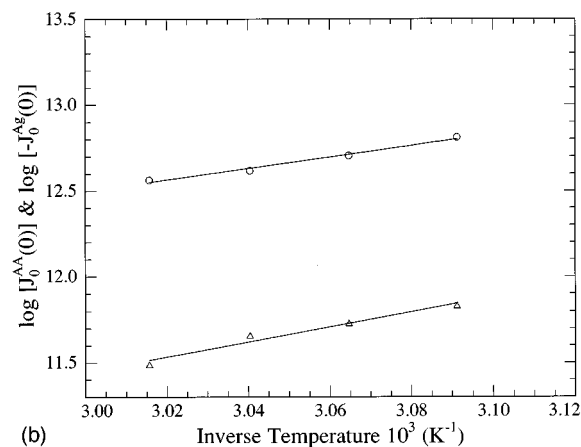
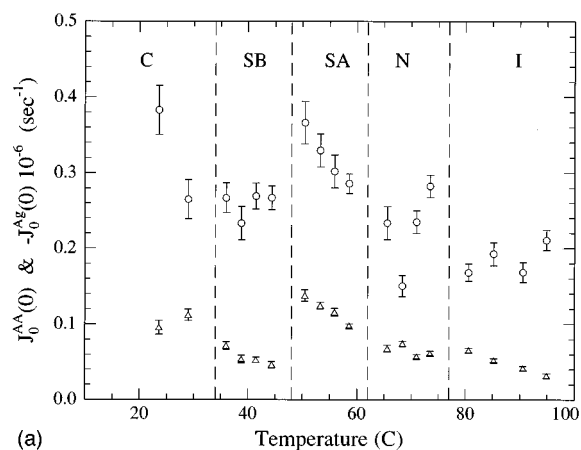


FIG. 4. (a) $J_0^{AA}(0)$ (open circles) and $J_0^{Ag}(0)$ (open triangles) versus temperature. From COSY (through *A*, *B*, and *C*) and ELDOR (W_n) measurements. (b) $J_0^{AA}(0)$ (open circles) and $J_0^{Ag}(0)$ (open triangles) versus temperature in S_A phase, the solid lines representing the best Arrhenius fit. Activation energies: for $J_0^{AA}(0)$ it is 13.8 ± 1.2 kcal/mol and for $J_0^{Ag}(0)$ it is 18.3 ± 2.5 kcal/mol.

TABLE II. Zero frequency spectral densities for PDT in 4O,8 from orientation-dependent studies ($M=0,1,2$).

| Phase | T ($^{\circ}\text{C}$) | $-J_M^{AG}(0) \times 10^6$ (s^{-1}) | | | $J_M^{AA}(0) \times 10^6$ (s^{-1}) | | |
|-------|----------------------------|--|-------------------|-------------------|---|-------------------|-------------------|
| | | $M=0$ | $M=1$ | $M=2$ | $M=0$ | $M=1$ | $M=2$ |
| S_A | 57 | 0.109 ± 0.006 | 0.084 ± 0.008 | 0.104 ± 0.008 | 0.296 ± 0.015 | 0.141 ± 0.019 | 0.117 ± 0.019 |
| S_A | 51 | 0.093 ± 0.007 | 0.079 ± 0.009 | 0.104 ± 0.005 | 0.276 ± 0.019 | 0.143 ± 0.025 | 0.191 ± 0.025 |
| S_B | 42 | 0.071 ± 0.007 | 0.038 ± 0.009 | 0.089 ± 0.009 | 0.189 ± 0.006 | 0.000 ± 0.008 | 0.167 ± 0.009 |
| S_B | 37 | 1.0 ± 0.007 | 0.494 ± 0.009 | 0.67 ± 0.009 | 0.216 ± 0.015 | 0.000 ± 0.008 | 0.179 ± 0.018 |

following expressions, which are strictly valid only for low ordering:⁶

$$J_0(\omega, \Theta) = \frac{1}{4}(1 - 3 \cos^2 \Theta)^2 J_0(\omega) + 3 \cos^2 \Theta \sin^2 \Theta J_1(\omega) + \frac{3}{8} \sin^4 \Theta J_2(\omega), \quad (10)$$

$$J_1(\omega, \Theta) = \frac{3}{2} \cos^2 \Theta \sin^2 \Theta J_0(\omega) + \frac{1}{2} [(1 - 2 \cos^2 \Theta)^2 + \cos^2 \Theta] J_1(\omega) + \frac{1}{2} (1 - \cos^4 \Theta) J_2(\omega), \quad (11)$$

$$J_2(\omega, \Theta) = \frac{3}{8} \sin^4 \Theta J_0(\omega) + \frac{1}{2} (1 - \cos^4 \Theta) J_1(\omega) + \frac{1}{8} [(1 + \cos^2 \Theta) + 4 \cos^2 \Theta] J_2(\omega), \quad (12)$$

where the $J_i(\omega, \Theta)$ are the orientation dependent spectral densities, and Θ is the angle between the nematic director and the dc magnetic field. The values of $J_M^{AG}(0)$ and $J_M^{AA}(0)$ obtained from these expressions are given in Table II (further details are given in the next subsection). These angular dependent spectral densities are plotted in Fig. 5 for one temperature in the S_A phase (57 $^{\circ}\text{C}$) and in the S_B phase (37 $^{\circ}\text{C}$).

C. The 2D-ELDOR spectra: W_n and ω_{HE}

The 2D-ELDOR spectra at each temperature have some readily noticeable features (cf. Fig. 1). First of all, the spectral lines in the 2D map, including the auto-peaks (for which $f_1 = f_2$), are all very narrow. Second, the cross-peaks remain very weak even as T_m increases, particularly in the ordered mesophases (cf. below). The low temperature S_B phase shows the smallest cross-peaks at a given mixing time. These spectra in all the different phases also indicate that the double cross-peaks (i.e., those for which f_1 and f_2 correspond to $M_I = \pm 1$ and ∓ 1 respectively) are virtually absent for all mixing times, indicating that there is no appreciable Heisenberg spin-exchange between radicals at this concentration. In the absence of Heisenberg exchange, the evolution of cross-peaks is a direct measure of the nuclear spin relaxation rate, W_n (due to electron–nuclear dipolar interactions), which is normally expected to increase with decrease in temperature, consistent with an increase of the correlation times under motional narrowing conditions. Instead the opposite is observed.

The initial analysis of the 2D-ELDOR experiments was carried out with a view to estimating W_n and ω_{HE} , and to observe what changes, if any, occur with mixing time. The well-resolved nature of these spectra permits the determination of these quantities in terms of the peak volumes for the auto- and cross-peaks as developed by GRF. This requires the accurate determinations of the auto- and cross-peak vol-

umes as a function of mixing time. 2D linear prediction techniques based on singular value decomposition (LPSVD) were employed to reconstruct the experimental data in terms of Lorentzian components with known amplitude, resonant frequency, width and phase (the latter three quantities are with respect to both f_1 and f_2). The deconvoluted and filtered experimental data were used in this analysis. The optimum number of LP coefficients along t_1 were typically found to be about 34 with about 17 predicted frequencies, including noise components and artifacts, while those for t_2

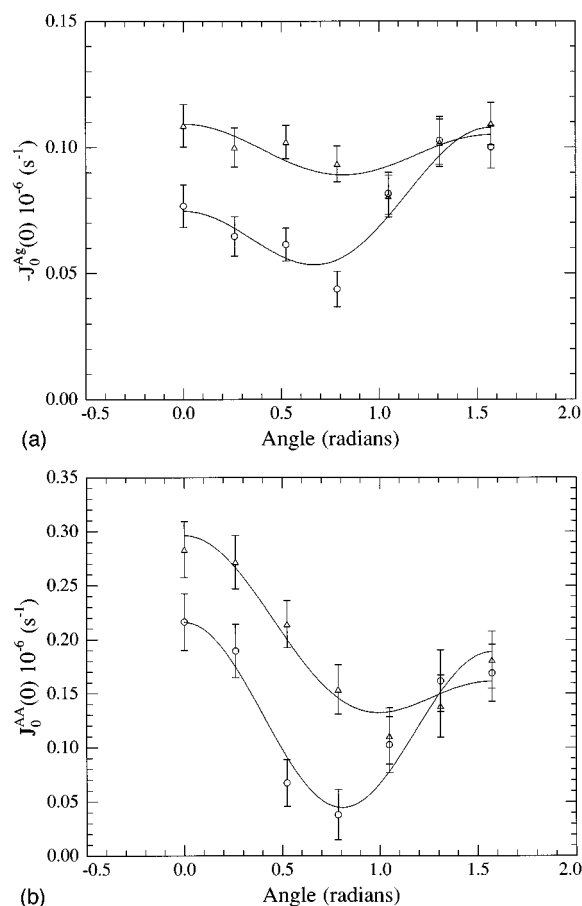


FIG. 5. (a) $J_0^{Ag}(0)$ versus director tilt in S_A phase (57 $^{\circ}\text{C}$; open triangles) and S_B phase (37 $^{\circ}\text{C}$; open circles), the solid lines represent the best fit in terms of $J_M^{AG}(0)$, $M=0, 1, 2$. (From orientation dependent COSY experiments.) (b) $J_0^{AA}(0)$ versus director tilt in S_A phase (57 $^{\circ}\text{C}$; open triangles) and S_B phase (37 $^{\circ}\text{C}$; open circles), the solid lines represent the best fit in terms of $J_M^{AA}(0)$, $M=0, 1, 2$. From orientation dependent COSY experiments.

were about 50 and 25, respectively. The predicted spectra consisted mainly of single Lorentzians at the coordinates of the auto- and cross-peaks in f_1, f_2 space, but the $M = -1$ (lowest frequency) auto-peak seemed to be better represented in a number of cases with a cluster of closely spaced Lorentzians (typically 2 or 3) instead. In those cases, appropriately integrated volumes were used to represent the total contribution in that region.

GRF give a set of 6 coupled linear equations involving the ratio of the 6 cross-peak volumes to respective auto-peak volumes, from which W_n and ω_{HE} may be obtained when nuclear-spin-dependent non-secular terms may be neglected. This overdetermined set of equations (i.e., 6 equations and 2 unknowns) may be solved by appropriate linear least squares methods.²³ In our present analysis the $\Delta M_I = \pm 1$ cross-peaks were measurable in all phases, but the $\Delta M_I = \pm 2$ cross-peaks were observable only in the isotropic phase. Thus for the isotropic phase all six coupled equations were used to extract both W_n and ω_{HE} , whereas in the ordered phases only four of these equations were utilized. In cases where $\omega_{\text{HE}} \approx 0$, then these equations can be replaced by a simpler analysis for just W_n . In particular, one has:

$$W_n = \frac{1}{6T_m} \ln \left(\frac{2\hat{Q}_{mj}V_j r_{2j} + V_m r_{2m}}{V_m r_{2m} - \hat{Q}_{mj}V_j r_{2j}} \right), \quad (13)$$

which applies just to the two cross-peaks for which $m = \pm 1$ and $j = 0$, and where \hat{Q} is the normalized matrix of 2D-ELDOR peak volumes [i.e., $\hat{Q}_{mj}(T) \equiv Q_{mj}(T)/Q_{00}(T)$ with $Q_{00}(T)$ the volume of the central auto-peak], and the products $V_j r_{2j}$ are the coverage corrections to each of the 3 hf lines determined from a single microwave pulse (i.e., FID) experiment. A somewhat more complex expression applies to the other two cross-peaks.

The volume data for all 6 to 8 mixing times at a given temperature were simultaneously used to get the optimum W_n and ω_{HE} . In the present analysis it was found that, whereas the spectrometer coverage corrections that are obtained from the single pulse FID experiment are fairly reliable, some variation of these parameters in the analysis in a least square sense provided a more accurate determination of the relaxation parameters. (Only $V_1 r_{2,1}$ and $V_{-1} r_{2,-1}$ need to be determined, since $V_0 r_{r,0}$ is conveniently set at unity.) The best fit values for these corrections are found to be close to the experimentally estimated results, typically within about 10%–15%. In the isotropic phase, the data are analyzed to yield both W_n and ω_{HE} . The value of ω_{HE} was found to be small. In the mesophases, ω_{HE} was found to be negligibly small, and hence only W_n could be measured in the N , S_A and S_B phases. Once W_n (and ω_{HE} in the isotropic phase) was determined, the decay of the auto- and cross-peak volumes, as a function of T_m , was analyzed to obtain the value of electron spin lattice relaxation rate (W_e), which was found to be essentially independent of temperature with a value of about $0.8\text{--}1 \times 10^6 \text{ s}^{-1}$. The variations of W_n (and ω_{HE} in the isotropic phase) with temperature are shown in Figs. 6(a) and 6(b). Note that W_n is observed from Fig. 6(a) to increase with decrease of T in the isotropic phase (as is typical), but it

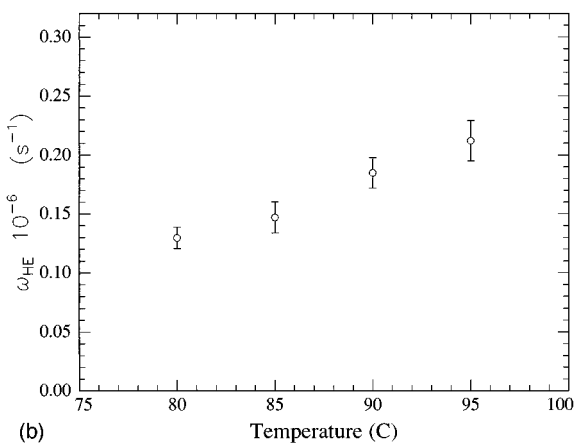
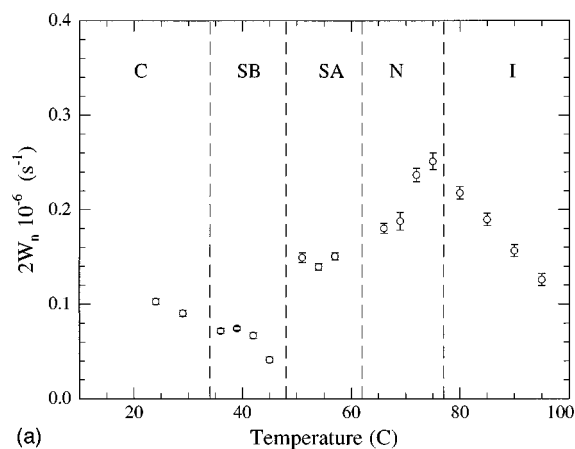


FIG. 6. (a) $2W_n$ versus temperature. From LPSVD based analysis of ELDOR data. (b) ω_{HE} versus temperature. From LPSVD based analysis of ELDOR data.

decreases with decreasing T in the N phase (on the face of it surprising). In the S_A phase it is smaller than in the higher temperature phases and it does not show significant changes with temperature. In the S_B and C phases, it is the smallest of all, though it exhibits a typical variation by increasing with decreasing temperature within each phase. The Heisenberg exchange measured for the I phase shows the expected decrease with T [Fig. 6(b)].

Initial experiments were performed to obtain orientation-dependent 2D-ELDOR spectra in the smectic phases, but it was difficult to obtain accurate cross-peak intensities, since they are intrinsically very small, and also the signal to noise posed some limitations. We did find that the already weak cross-peaks did decrease with orientation Θ , but did not appear to exhibit a large variation with angle. Thus we did not attempt any detailed quantitative studies. In order to estimate $J_0^{AA}(0, \Theta)$ from Eq. (7) we utilized the fact that W_n is considerably smaller than C in the S_A and S_B phases to add $W_n(\Theta = 0)$ to $C(\Theta)$. Given that W_n is observed to decrease for $\Theta \neq 0$, the $J_0^{AA}(0, \Theta)$ estimated in this fashion are ex-

pected to be a little larger than the true values for $\Theta \neq 0$, and this affects the $J_M^{AA}(0)$ in Table II and Fig. 5(b).

D. Global fitting of the 2D-ELDOR spectra to microscopic dynamic models

Instead of the phenomenological approach of determining the various relaxation rates (i.e., the linewidths and the W_n and ω_{HE} values) and then analyzing them to yield the spectral densities associated with the spin relaxation, a more global approach is available to us. In this approach, a particular microscopic model for the dynamic molecular processes is directly fit to the complete set of 2D-ELDOR spectra (for the different T_m) at a given temperature yielding best-fit values for the parameters, and an assessment can be made of the degree to which the microscopic model is successful in fitting the results. In this way, the effects of microscopic models of the 2D FT-ESR spectra may be determined directly via the stochastic-Liouville equation (SLE), and all key spectral features are fit simultaneously without the need to partition the effect upon each spectral density term from the model. Of course, in the slow-motional regime it would not even be possible to extract simple spectral densities from the experiment, and such a global approach is the only practical one. Thus, we had to use such an approach in analyzing the present results of CLS in 4O,8, and for the reasons just stated, it would appear sensible to employ the same approach for analyzing the present results of PDT in 4O,8.

Additional advantages of this global approach are: the full set of 2D-ELDOR spectra with different mixing times are used, and they contain more extensive (homogeneous) line shape information for the auto- and cross-peaks than just a single COSY spectrum, as well as the cross-relaxation (i.e., W_n and ω_{HE}) information. Also, to utilize sophisticated microscopic models such as SRLS, it would be necessary to calculate from the models a variety of reorientational spectral density terms instead of computing their composite effect on the 2D spectrum. Finally, we allow for the possibility of any slow motional effects from, e.g., a slowly relaxing dynamic cage. (Note that in the limit of a very slowly reorienting cage one achieves a MOMD spectrum which is characterized by substantial inhomogeneous broadening. Our LPSVD-based COSY studies did in fact indicate that the $M_I = -1$ line, which is the broadest, could be better represented by 2 or 3 Lorentzians, rather than a single Lorentzian, in a number of cases.)

A significant technical problem arose in dealing with the 2D-FT-ESR spectra with narrow lines arising from the feature of the FFT that the frequency resolution is essentially determined by $1/\Delta t$, where Δt is the length of the time domain signal. The values of Δt_1 and Δt_2 that we used did not provide adequate frequency resolution for discriminating the sharp lines. However, this problem was easily overcome, as noted in Sec. II, by zero-filling the data sets to double the values of Δt_1 and Δt_2 (i.e., the original data set of density 128×256 points was thereby increased to 256×512 points). Note that such a problem would not have existed if we had

chosen to work with the linear predicted data set, but we felt it would be more reliable to utilize the original data set to avoid any approximations or artifacts introduced by the LPSVD.

The presence of very weak and narrow cross-peaks presented another problem for utilizing non-linear least squares (NLLS) methods to fit the experimental spectra by simulations. Due to the relatively more intense auto-peaks, simple implementation of the NLLS fitting procedures tended to ignore the features of the cross-peaks in favor of the features of the auto-peaks. This required an acceptable procedure for enhancing the relative importance of the weak cross-peaks. This was accomplished by weighting both the experimental and computed 2D-FT-ESR spectra such that the role of the four $\Delta M = \pm 1$ cross-peaks was enhanced. We used 2D Gaussian weighting functions with a width that encompassed each cross-peak and an amplitude that increased the intensity of these cross-peaks by a factor of 5. The data at all the mixing times (at a given temperature) were included simultaneously in these NLLS fittings. In order to compensate for the loss of intensity of these spectra with mixing time [due to electron spin lattice relaxation (T_{1e}) processes], the highest auto-peak in the 2D spectrum for each mixing time is normalized to unity. Thus, each such spectrum was given about equal weight in the fitting. (Of course the 2D spectra for longer mixing times, with their decreased S/N, thereby introduced more noise into the fitting.) This scheme is found to be very helpful in fitting the present data in a fashion that takes proper heed of the importance of the cross-peak development with mixing time.

The set of 2D-ELDOR spectra for the different mixing times, T_m , at each temperature were fitted to the SRLS model (cf. Paper I). For purposes of comparison, the spectra were also fitted to the standard model of Brownian reorientation in a macroscopic orienting potential (cf. Paper I) for a single temperature in each phase. Typical results of these simulations are shown in Fig. 7 for just two of the 6–8 values of T_m for economy in presentation. Also, we show results for just the one temperature in each phase for which calculations were also performed with the standard model. In all phases the best fit to the SRLS model is seen to be superior to that of the standard model. In all phases, save the nematic, the SRLS model provides a very good overall fit to the intensities and widths of the auto- and cross-peaks. The nematic phase is a special case because of large additional contributions to the spin relaxation due to quasi-critical fluctuations associated with the nearby $I-N$ and $N-S_A$ phase transitions.^{5,24} We have not attempted to correct for these additional dynamic processes and simultaneously fit to the SRLS model. Thus, we consider our results for the N phase as being less reliable than those for the other phases.

We also examined the effect of preferentially weighting the cross-peaks in performing the NLLS fits by varying the weighting factor. We found that within the estimated uncertainties in the fits, the results using the SRLS model were typically not significantly changed. However, for the standard model, this was not the case. With substantial weighting

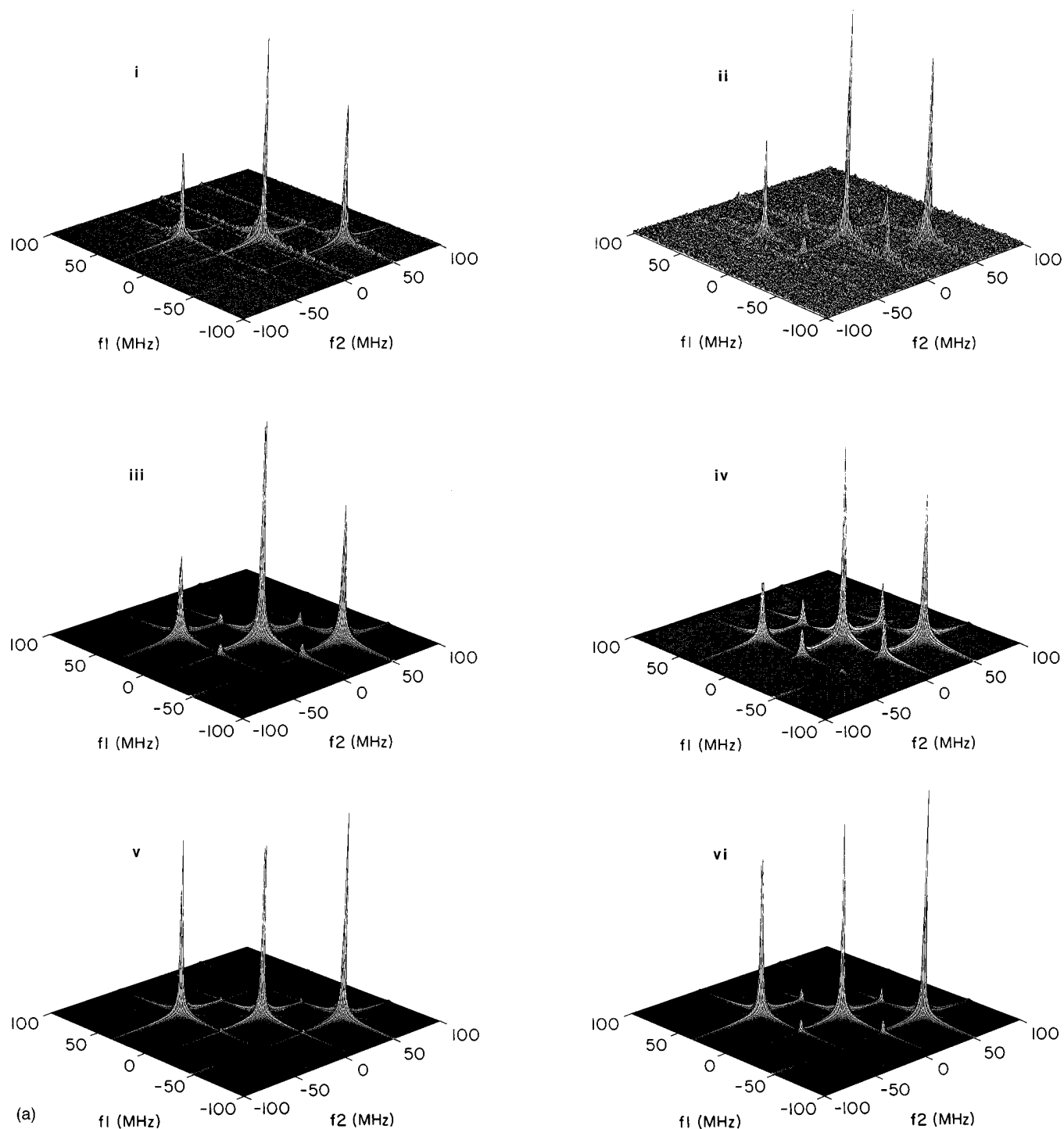


FIG. 7. Simulated 2D-ELDOR spectra based on SRLS and standard (Simple) models compared with experimental spectra at representative temperatures in each phase: (a) 90 °C—*I*; (b) 72 °C—*N*; (c) 57 °C—*S_A*; (d) 39 °C—*S_B*; (e) 24 °C—*C*. In (a)–(d), the spectra labelled (i) and (ii) are experimental for $T_m = 400$ ns [300 ns for (a)] and 1000 ns respectively; those labelled (iii) and (iv) represent the respective SRLS fits; those labelled (v) and (vi) represent the respective “standard” fits. In (e), (i)–(iii) are the experimental spectra for $T_m = 400, 800,$ and 1000 ns, respectively and (iv)–(vi) are their respective SRLS fits. Because of the reduction in the size of these 2D spectra, the weak cross-peaks are more clearly seen in the simulations; but they are observed at the same coordinates in the experimental spectra. (a) is shown above and (b)–(e) are shown on subsequent pages.

of the cross-peaks, their intensities are fit reasonably well, but the relative heights of the auto-peaks are not when the standard model was used, as seen in Fig. 7. When the cross-peaks are not weighted in the fits, then the reverse is the case. This is most likely a consequence of the use of a model

which is not very satisfactory, viz. the standard model.

The results of the 10-parameter SRLS fits for all temperatures are given in Table III, and those for the 7-parameter standard fits appear in Table IV. [In the *I* phase an additional fitting parameter is ω_{HE} , but a_0^2 and a_2^2 are

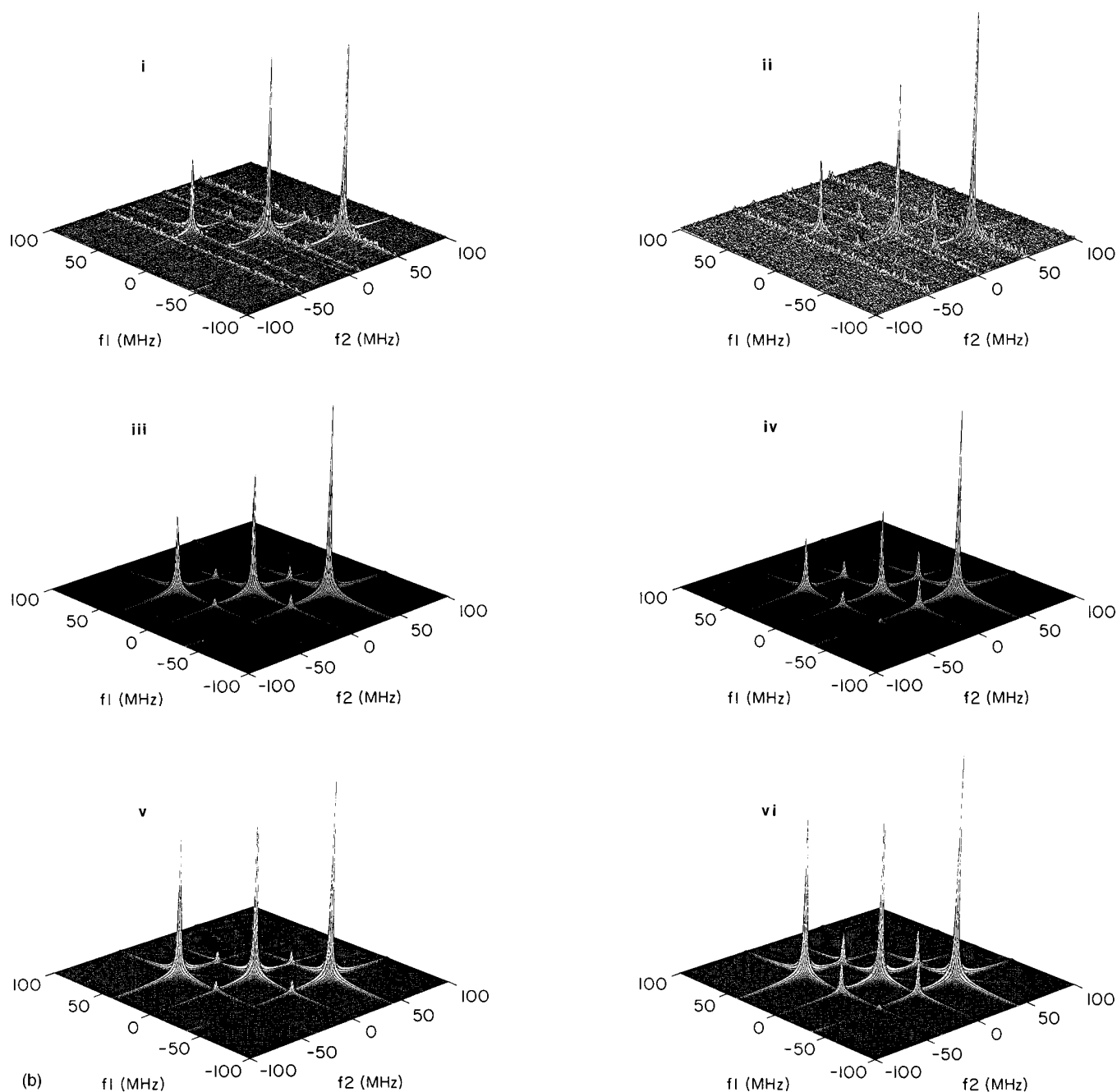


FIG. 7(b). See caption to Fig. 7(a).

zero. The results on ω_{HE} are close to those shown in Fig. 6(b), so we do not list them in Table III.] In principle [cf. Eq.(43) of Paper I] the probe potential coefficients a_0^2 and a_2^2 (defined in Eq. (10) of Paper I) are derivable from the values of $\langle \mathcal{S}_{00}^2(\Omega^0) \rangle$ and $\langle \mathcal{S}_{02}^2(\Omega^0) + \mathcal{S}_{0-2}^2(\Omega^0) \rangle$ given in Fig. 3.⁶ We adopted the procedure of using the values of a_0^2 and a_2^2 obtained in this manner as seed values for the NLLS fits. The final values of a_0^2 and a_2^2 were only slightly modified by the NLLS procedure but did improve the fits somewhat. The reason why we chose not to reduce our fitting parameters by two is that the set of 2D-ELDOR spectra for 6–8 mixing times provides much greater independent data

on the line positions (which directly reflect the macroscopic ordering) from both auto- and cross-peaks than does a single FID spectrum. (Also, there are expected small corrections to the order parameters measured from the line positions due to the presence of a local structure [GRF].)

Note that the theoretical constraint, $T_{1e} \geq T_{2e}$, is obeyed in virtually all our fits (the one exception, for 57.4°C in the S_A phase, has $T_{1e} \approx T_{2e}$ within experimental error). The values of T_{1e} are found to be of the order of 0.5 μs without very much variation in the different phases. [These values are in good agreement with the $T_{1e} \equiv (2W_e)^{-1}$ found from the integrated auto- and cross-peak volumes using LPSVD meth-

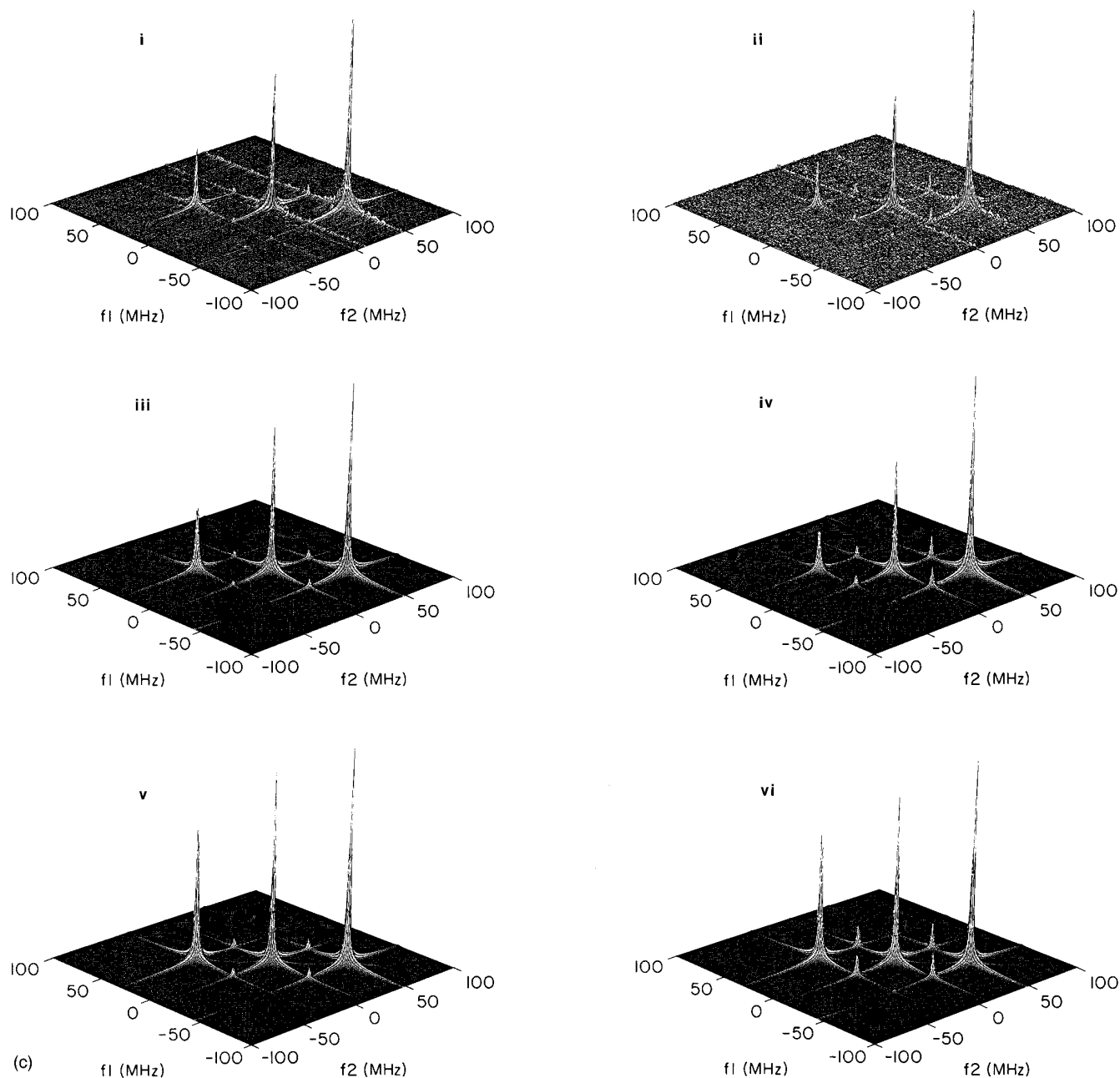


FIG. 7(c). See caption to Fig. 7(a).

ods, cf. above.] The fact that T_{1e} is typically nearly comparable to T_{2e} is consistent with a single spin-relaxation mechanism being dominant for both, and the expected mechanism for which $T_{1e} \approx T_{2e}$ is spin-rotational relaxation.^{6,2} Note also that the Gaussian inhomogeneous broadening parameter Δ_G is small, about 0.1 G, and essentially temperature independent, as expected for a perdeuterated spin probe that is weakly ordered.

Our primary interest is in the rotational diffusion of the PDT probe, given by $\bar{R}^o \equiv \sqrt{R_\perp^2 R_\parallel}$, and $N \equiv R_\parallel / R_\perp$ (where R_\perp and R_\parallel are respectively the perpendicular and parallel components of the rotational diffusion tensor), the rotational diffusion coefficient of the cage, R^c , and the cage potential

parameters, c_0^2 and c_2^2 , defined by Eq. (12) of Paper I. The latter are plotted as a function of temperature in Fig. 8(a), and the local order parameters $S_{l,0}^2 = \langle \mathcal{L}_{0,0}^2(\Omega) \rangle$ and $S_{l,2}^2 = \langle \mathcal{L}_{0,2}^2(\Omega) + \mathcal{L}_{0,-2}^2(\Omega) \rangle$ derivable from them according to Eq. (44) of Paper I are plotted in Fig. 8(b). The cage potential coefficient c_0^2 remains at about $1k_B T$ (in dimensional units) through the I , N , and S_A phases, dropping slightly in the S_B phase, but returning to about $1k_B T$ in the C phase. There is a gradual increase in c_0^2 with decreasing T , but a drop in its value for the C phase. The order parameters show similar behavior, as expected. The cage potential parameters c_0^2 and c_2^2 are found to be larger than the macroscopic orienting potential coefficients a_0^2 and a_2^2 , with a_0^2

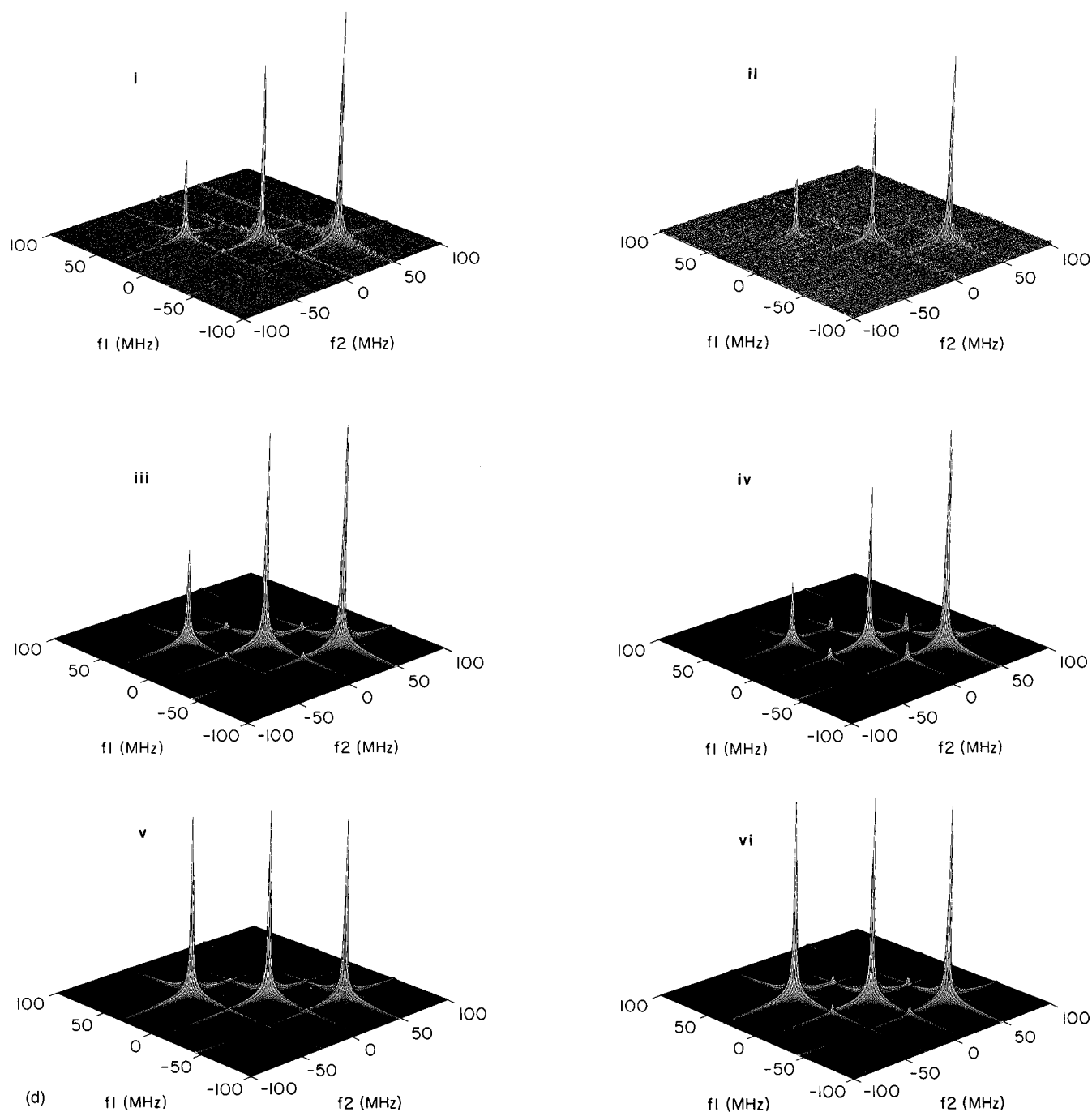


FIG. 7(d). See caption to Fig. 7(a).

ranging from about $0.1k_B T$ in the N phase and increasing to about $0.3k_B T$ in the S_B phase. The asymmetry coefficient a_2^2 decreases to nearly zero even as a_0^2 increases with decreasing T . On the other hand, c_2^2 , while smaller than c_0^2 , remains substantial, except in the isotropic phase where it is close to zero.

The diffusion coefficients \bar{R}^o and R^c plotted in Fig. 9 are seen to fall in the range of 10^{10} s^{-1} and 10^8 s^{-1} respectively. Thus, the cage is seen to relax about two orders of magnitude slower than the PDT probe. In fact, these values of R^c are typically in the incipient slow-motional regime.

The anisotropy in the R^o tensor is small and fairly constant over temperature with $N \approx 2$, consistent with previous studies on PDT.⁶ [In this study we are neglecting any small difference $(R_{x'x'}^o - R_{y'y'}^o)$ compared to the mean $\frac{1}{2}(R_{x'x'}^o + R_{y'y'}^o) = R_{\perp}$.]²⁵ Note that within each phase \bar{R}^o decreases somewhat with decreasing T , except for the S_A phase, where it appears to remain constant (and for a point in the I phase near the $I-N$ transition, which is clearly a manifestation of the quasi-critical effects associated with this transition). Somewhat related thermal behavior is noted for R^c ,

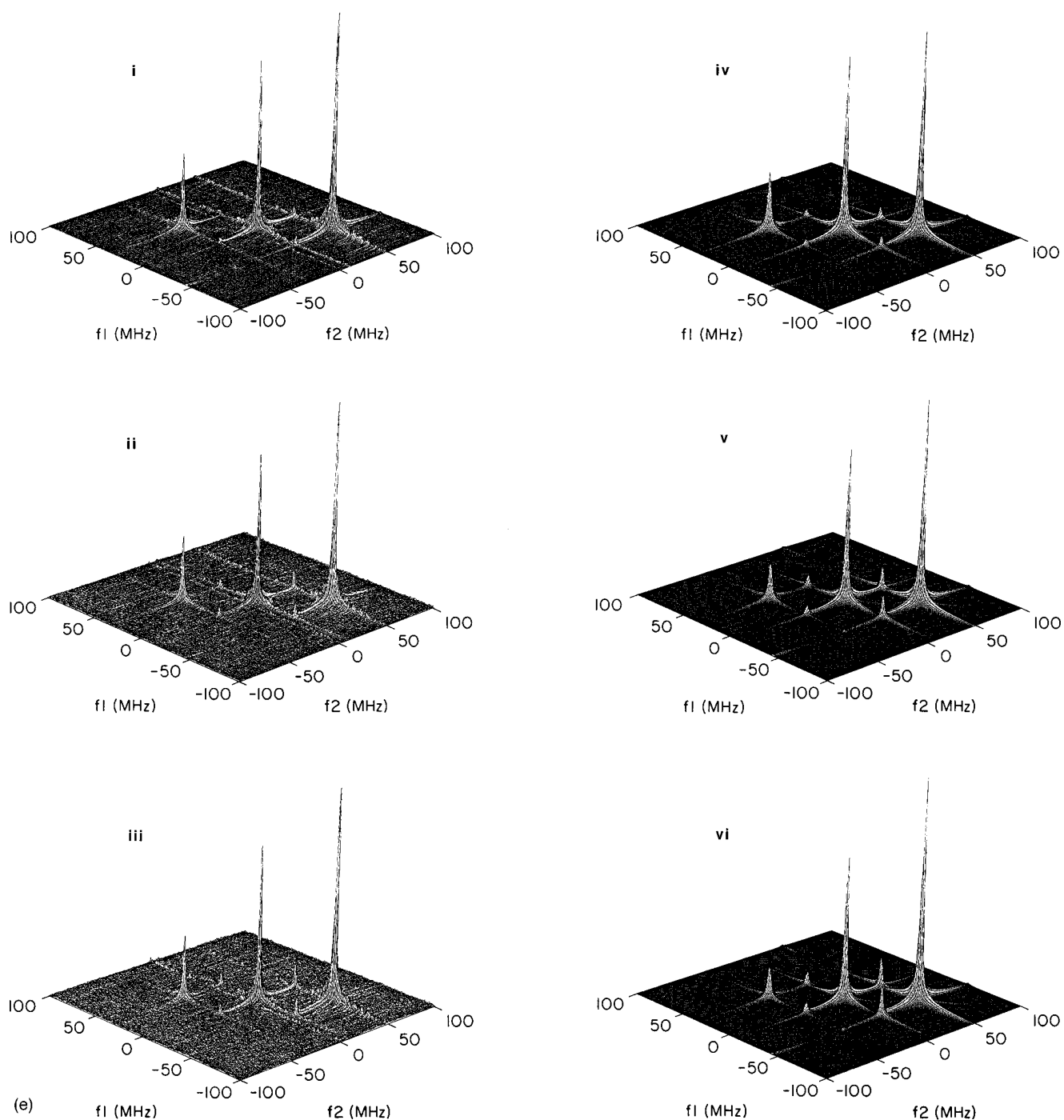


FIG. 7(e). See caption to Fig. 7(a).

except for the N phase (and the same anomalous point in the I phase). We expect that these results in the N phase are significantly corrupted by the quasi-critical effects due to both the $I-N$ and $N-S_A$ transitions, so we shall ignore them in our subsequent discussion.

When we compare the results of Table IV for the analysis based on the standard model with those of Table III for the SRLS model we find that \bar{R}^o is a little smaller for the former (ranging from 50% to 75%), while N remains close to 2. The macroscopic orientational parameters are nearly the

same, while T_{1e} and T_{2e} are slightly shorter for the standard model. The reduction in \bar{R}^o for the standard model is required to compensate for the absence of the SRLS contribution to the linewidths and the W_n 's.

E. Non-secular terms

As in the previous study of GRF, we have neglected nuclear spin dependent non-secular terms arising from motional averaging of the electron-nuclear dipolar and g -tensor

TABLE III. Optimum parameters obtained from fits to the SRLS model.^a

| T (°C) phase | $\bar{R}^o \times 10^{-10}$ (s ⁻¹) | N | a_0^2 | a_2^2 | $T_{1,e}$ (in μ s) | $T_{2,e}$ (in μ s) | Δ_G (G) | c_0^2 | c_2^2 | $R^c \times 10^{-8}$ (s ⁻¹) |
|-------------------------------|--|------|---------|---------|------------------------|------------------------|----------------|---------|---------|---|
| 94.6 (<i>I</i>) | 1.01 | 2.27 | ... | ... | 0.583 | 0.493 | 0.079 | 1.04 | -0.060 | 0.42 |
| 89.8 (<i>I</i>) | 0.85 | 2.02 | ... | ... | 0.574 | 0.388 | 0.095 | 1.08 | -0.025 | 0.31 |
| 84.7 (<i>I</i>) | 0.54 | 2.29 | ... | ... | 0.446 | 0.426 | 0.099 | 1.08 | -0.056 | 0.13 |
| 79.8 (<i>I</i>) | 1.07 | 2.25 | ... | ... | 0.479 | 0.363 | 0.129 | 1.03 | 0.13 | 0.46 |
| 75.2 (<i>N</i>) | 1.00 | 2.00 | 0.036 | 0.226 | 0.516 | 0.452 | 0.094 | 1.01 | 0.32 | 0.74 |
| 72.3 (<i>N</i>) | 0.71 | 1.77 | 0.103 | 0.228 | 0.485 | 0.437 | 0.067 | 1.09 | 0.25 | 2.10 |
| 69.4 (<i>N</i>) | 0.71 | 2.03 | 0.153 | 0.227 | 0.558 | 0.429 | 0.070 | 1.11 | 0.27 | 2.66 |
| 65.8 (<i>N</i>) | 0.47 | 1.81 | 0.241 | 0.223 | 0.486 | 0.375 | 0.069 | 1.10 | 0.33 | 9.96 |
| 60.0 (<i>S_A</i>) | 1.39 | 2.20 | 0.220 | 0.218 | 0.558 | 0.527 | 0.108 | 1.00 | 0.26 | 1.00 |
| 57.4 (<i>S_A</i>) | 1.40 | 1.70 | 0.236 | 0.208 | 0.486 | 0.526 | 0.104 | 1.02 | 0.23 | 1.18 |
| 54.2 (<i>S_A</i>) | 1.38 | 2.00 | 0.224 | 0.196 | 0.644 | 0.532 | 0.063 | 1.12 | 0.31 | 0.91 |
| 50.5 (<i>S_A</i>) | 1.38 | 2.00 | 0.239 | 0.184 | 0.701 | 0.527 | 0.072 | 1.11 | 0.33 | 1.05 |
| 44.5 (<i>S_B</i>) | 3.18 | 2.06 | 0.238 | 0.039 | 0.679 | 0.436 | 0.102 | 0.82 | 0.44 | 0.86 |
| 41.8 (<i>S_B</i>) | 3.16 | 2.10 | 0.249 | 0.037 | 0.550 | 0.451 | 0.093 | 0.79 | 0.45 | 1.75 |
| 38.8 (<i>S_B</i>) | 2.72 | 2.14 | 0.318 | 0.012 | 0.601 | 0.436 | 0.100 | 0.73 | 0.46 | 1.20 |
| 35.8 (<i>S_B</i>) | 2.45 | 1.90 | 0.334 | 0.013 | 0.634 | 0.450 | 0.110 | 0.74 | 0.45 | 1.09 |
| 29.1 (<i>K</i>) | 1.26 | 2.02 | 0.271 | 0.056 | 0.759 | 0.421 | 0.121 | 1.06 | 0.17 | 1.85 |
| 24.2 (<i>K</i>) | 1.30 | 2.00 | 0.227 | 0.071 | 0.714 | 0.449 | 0.123 | 1.12 | 0.23 | 1.47 |

^aThe average percent errors to the parameters are $\epsilon_{\bar{R}^o}=3.8$, $\epsilon_N=1.8$, $\epsilon_{a_0^2}=2.7$, $\epsilon_{a_2^2}=5.0$, $\epsilon_{T_{1,e}}=6.0$, $\epsilon_{T_{2,e}}=5.0$, $\epsilon_{\Delta_G}=4.0$, $\epsilon_{c_0^2}=6.5$, $\epsilon_{c_2^2}=10$, $\epsilon_{R^c}=9.0$.

interactions, requiring *a posteriori* justification. In their original cw-ESR study of PDT in 4O,8, Lin and Freed (LF)³ considered the possibility of non-negligible non-secular contributions to the *A*, *B*, and *C* linewidth terms in the isotropic phase. Following PF,² they pointed out that the data required a suppression of the non-secular spectral densities, for example by the use of a modified spectral density function $\tau_R/(1+\epsilon\tau_R^2\omega_0^2)$ with the adjustable parameter $\epsilon>1$, and they obtained $\epsilon=7\pm 1$ (or alternatively unreasonably large rotational asymmetries for PDT were required). In the present study, wherein we have separated $J_1^{AA}(\omega_a)$ and $J_0^{AA}(0)$ from the *C* linewidth term and W_n , we have additional evidence of the relative unimportance of the non-secular terms. Thus, our analysis, neglecting non-secular contributions to *C* and W_n , resulted in $J_1^{AA}(\omega_a)\approx J_0^{AA}(0)$ in the isotropic phase. This is an appropriate result given that $J_M(\omega)$ must be independent of *M* due to the spatial isotropy and also $\omega_a^2\tau_R^2\ll 1$ where $\omega_a/2\pi$ is the nuclear-spin flip frequency. If non-secular contributions were significant (but are neglected in our analysis) then the apparent (but incorrect) values of $J_1^{AA}(\omega_a)$ and $J_0^{AA}(0)$ would not be equal because these non-secular terms affect *C* and W_n differently. Neglecting the *M* subscript we can write $C\cong\frac{8}{3}J^{AA}(0)-J^{AA}(\omega_a)-\frac{1}{3}J^{AA}(\omega_e)$, so *C* is slightly reduced by the non-secular term. Using the perturbation analysis of GRF for the effects of non-secular terms on 2D-ELDOR, one must consider the difference between the two normal mode decay

rates τ_3^{-1} and τ_1^{-1} . In the absence of non-secular terms (and $\omega_{HE}\approx 0$), we have $\tau_3^{-1}-\tau_1^{-1}=6W_n$.⁴ When they are non-negligible $\tau_3^{-1}-\tau_1^{-1}\cong 6W_n-6J^{AA}(\omega_e)=3J^{AA}(\omega_a)-6J^{AA}(\omega_e)$. Thus our procedures would lead to an estimated $J^{AA}(\omega_a)^{est}=2W_n^{est}=J^{AA}(\omega_a)-2J^{AA}(\omega_e)$, and then to a $J^{AA}(0)^{est}=\frac{3}{8}C+\frac{3}{8}J^{AA}(\omega_a)^{est}=J^{AA}(0)-\frac{7}{8}J^{AA}(\omega_e)$. For appreciable values of $J^{AA}(\omega_e)/J^{AA}(0)\cong J^{AA}(\omega_e)/J^{AA}(\omega_a)$, the $J^{AA}(\omega_a)^{est}$ would be significantly smaller than the $J^{AA}(0)^{est}$.²⁶ In the nematic phase we still observe a $J_1^{AA}(\omega_a)\approx J_0^{AA}(0)$, but the analysis becomes more complex.

Ultimately, (as in GRF) we rely on a self-consistency in our analysis. In particular, we look to the SRLS mechanism to suppress the contribution of non-secular terms. That is, the effect of SRLS can be very roughly approximated by letting the Debye spectral density function, $\tau_R/(1+\omega^2\tau_R^2)$, be replaced by $[1-S_l^2]\tau_R/(1+\omega^2\tau_R^2)+S_l^2\tau_c/[1+\omega^2\tau_c^2]$,⁶ [where $\tau_R\equiv(6R^o)^{-1}$ and $\tau_c\equiv(6R^c)^{-1}$, and $S_l^2\equiv(S_{l,0}^2)^2$] and we find from our analyses that the ‘‘cage term’’ (i.e., the one in S_l^2) accounts for about 75% of the contributions to *B* and *C* in both the *I* and *S_A* phases. Then with the values of S_l^2 , τ_R and τ_c from Table III, we estimate errors in $J_0^{AA}(0)$ and $J_1^{AA}(\omega_a)$ of about 2.2% and 5.1%, respectively, arising from neglect of non-secular terms. This is well within the uncertainties of our detailed analyses. (In our opinion, the most effective way to deal with the non-secular contributions would be to perform frequency-dependent 2D-ELDOR ex-

TABLE IV. Optimum parameters obtained from fits to the standard model.

| Phase | T (°C) | $\bar{R}^o \times 10^{-10}$ (s ⁻¹) | N | a_0^2 | a_2^2 | $T_{1,e}$ (in μ s) | $T_{2,e}$ (in μ s) | Δ_G (G) |
|----------------------|----------|--|-----|---------|---------|------------------------|------------------------|----------------|
| <i>I</i> | 94.6 | 0.50 | 2.0 | ... | ... | 0.451 | 0.328 | 0.122 |
| <i>N</i> | 72.3 | 0.54 | 2.0 | 0.147 | 0.204 | 0.377 | 0.393 | 0.100 |
| <i>S_A</i> | 57.4 | 0.74 | 2.0 | 0.250 | 0.197 | 0.382 | 0.451 | 0.127 |
| <i>S_B</i> | 38.8 | 2.11 | 2.0 | 0.334 | 0.010 | 0.403 | 0.294 | 0.094 |

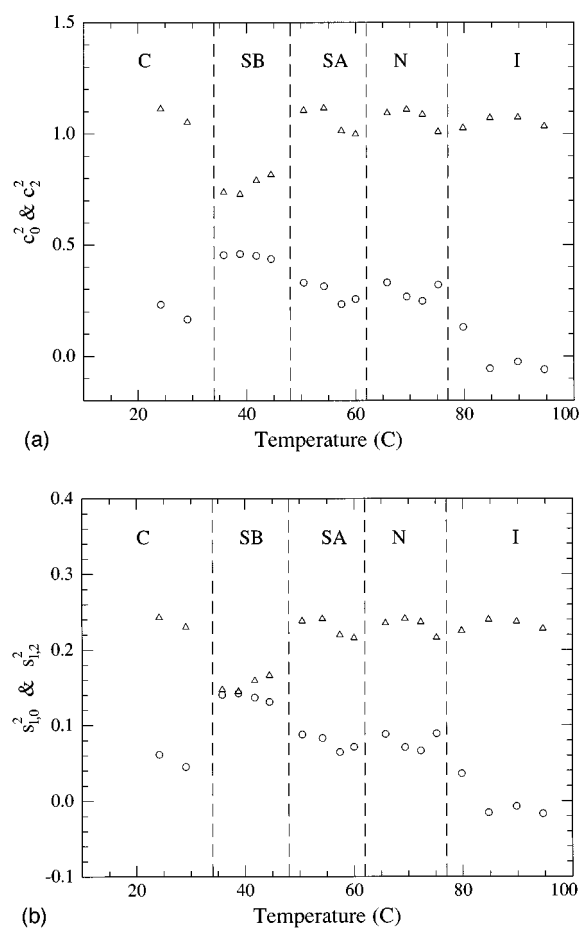


FIG. 8. (a) Potential parameters due to cage versus temperature (from SRLS based simulations). Open circles represent c_0^2 and open triangles represent c_2^2 . (b) Local order parameters due to cage versus temperature (from SRLS based simulations). Open circles represent $S_{l,0}^2 = \langle \mathcal{P}_{00}^2(\Omega) \rangle$ and open triangles represent $S_{l,2}^2 = \langle \mathcal{P}_{02}^2(\Omega) + \mathcal{P}_{0-2}^2(\Omega) \rangle_l$.

periments. We are currently constructing a 17 GHz 2D-ELDOR bridge, which would make such experiments feasible. Higher frequencies will, of course, suppress non-secular contributions.)

On another matter, we pointed out in Paper I that the hydrodynamic model of director fluctuations, which is important in nuclear magnetic resonance (NMR) relaxation, is too slow and too weak to be of importance in ESR as discussed previously.^{2,6} Our observations that $J_1^{AA}(\omega_a) \approx J_0^{AA}(0)$ in the N phase, and that $J_1^{AA}(\omega_a) = 2W_n$ is very small in all phases, are consistent with this conclusion, since it is the $J_M(\omega)$ spectral density with $M = \pm 1$ that is primarily affected by this mechanism and not the $M = 0$ spectral density.^{2,24}

IV. DISCUSSION

We first reconsider the unusual variation, with liquid crystal phase, of the 2D-ELDOR spectra that are illustrated in Fig. 1. The cross-peaks remain small (about 6 times smaller than for PDT in the smectic S₂),⁴ characteristic of very rapid motion. This confirms the conclusions of LF who

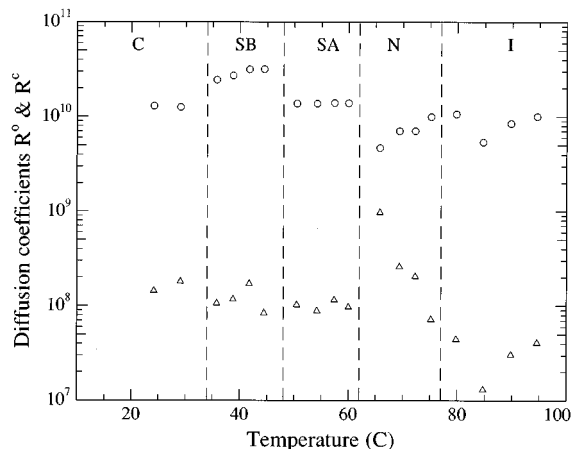


FIG. 9. Average rotational diffusion coefficients of the probe (open triangles) and of the cage (open circles) versus temperature. From SRLS based simulations.

just studied the cw-ESR linewidths. However, unlike their interpretation that large changes were occurring in $\tau_R (\equiv 1/6\bar{R}^o)$ with changes in phase, (e.g., a factor of nearly 5 decrease in τ_R as the temperature is lowered from the S_A into the S_B phase) we find that the τ_R remains more nearly the same from our NLLS fits of the SRLS model to the 2D-ELDOR data. This model allows for a moderate drop in the strength of the local structure at the S_A to S_B transition, which reduces the magnitude of both the linewidths and the cross-peaks, without requiring the large drop in τ_R . Most significant, the SRLS model leads to rather good fits in the various phases, whereas the standard model is unsuccessful. This provides good support of the postulate of a SRLS mechanism by LF, and the 2D-ELDOR significantly dramatizes the failure of the standard model.

It is also important that we are able to quantify the details of the SRLS model utilizing the NLLS fits to the 2D-ELDOR experiments. Study of just the cw-ESR linewidths did not permit this, nor could they be regarded as completely accurate, because of residual inhomogeneous broadening. We find that the cage potential has only a moderate effect on the motion of the PDT with local order parameters of about 0.25 and with asymmetry increasing with decreasing temperature. Both \bar{R}^o and R^c do not show marked temperature dependence. These features are fully consistent with LF who concluded that in the smectic phases there is “a (partial) expulsion of the PDT from the dipolar region of the liquid-crystalline molecules (which is preferred by the polar PDT molecule) toward the more flexible hydrocarbon end chains as a result of the packing of the smectic layers.” Furthermore they interpret their observations “in terms of a SRLS model due to the slow fluctuations of the hydrocarbon chains.” Our present analysis shows that this process is a fairly continuous one starting even in the isotropic phase. The lack of substantial temperature dependence in \bar{R}^o , R^c , and $S_{l,0}^2$ may be interpreted by this expulsion effect. The lower the temperature and phase, the more the PDT experiences the less confined aliphatic chain region, which tends to offset the usual effects of reduced temperature. LF dealt with

what appeared to them a large increase in \bar{R}^o at the $S_A \rightarrow S_B$ transition (cf. previous paragraph) as due to “a partial freezing (or slowing down) of the hydrocarbon end chains at the $S_A \rightarrow S_B$ transition such that the PDT is in a fairly well-defined cavity with reduced ‘frictional’ restriction to its motion, so its τ_R decreases.” Instead, in this work we have seen that this partial freezing reflects itself in somewhat reduced local ordering and a more moderate decrease in τ_R .

When we compare the results on PDT in 4O,8 with those on CSL in 4O,8 reported in Paper I, we note significant differences. The cage potential for CSL becomes very substantial mainly in the N and S_A phases with order parameters $S_{I,0}^2$ ranging from 0.4 to 0.5. The drop in cage potential at the $S_A \rightarrow S_B$ transition is much more dramatic for CSL. Of course \bar{R}^o for PDT is much faster than is R_{\parallel}^o and R_{\perp}^o for CSL (typically one (two) orders of magnitude faster for PDT than for R_{\parallel}^o (R_{\perp}^o) of CSL) as expected for the small PDT probe, which can effectively seek out the voids or regions of free volume existing in the liquid crystalline phases. Most interesting is a comparison of R^c as seen by the two spin probes. One finds that at the highest temperatures (i.e., the I phase) R^c for PDT is a few times larger than for CSL (e.g. about twice at 95 °C and about thrice at 85 °C). However in the smectic phases the values of R^c differ greatly. In the S_A phase they differ by a factor of 30–40, and in the S_B phase their ratio increases to a factor of about 500 or more. All these differences are consistent with our model that includes the different way these two probes sample their environment. The CSL is affected by the overall dynamic structure of the liquid crystal, whereas PDT is sensitive to its precise location relative to the liquid crystal molecules, and this changes with the phase. At the high temperatures the PDT is near the aromatic cores and therefore experiences a cage not unlike that of CSL, whereas in the smectic phases, CSL experiences the slower overall motions of the surrounding liquid crystal molecules, but PDT has moved deeper into the aliphatic chain region where more rapid fluctuations can occur. This is most dramatic in the S_B phase in which the overall motion has nearly frozen out but (collective) hydrocarbon chain fluctuations are still permitted.

When we compare the present results to those obtained by GRF on PDT in the S_A phase of S2, most prominent is the weak cross-peaks in the present study such that W_n is 6–8 times smaller. LF had previously argued that the expulsion effect as T decreases is less important for cyanobiphenyls, so the motion of PDT is slower in S2. We can best compare the results of the 2 experiments in terms of the spectral densities for the S_A phase. First we note that the ratio $-J_0^{Ag}(0)/J_0^{AA}(0)$ is constant at 0.38 in this phase, and this is very close to the near constant value of 0.40 obtained for PDT in S2 in the S_A phase. The present study, however, shows that this constancy is not preserved in the other phases. This ratio can be varied by changing the relative importance of c_{22} vs c_{20} , the local structure aligning potentials, as well as by varying R^c . (It is also affected by the values of a_{20} , a_{22} , and N .) The ratio of $J_0^{AA}(0)/J_1^{AA}(\omega_a)$,

which is unity in the I phase as it should be (cf. Sec. II), ranges from 2.0 to 2.5 in the S_A phase as T decreases. For PDT in S2, this ratio was found to go from unity to about 2 with decrease in T . This decrease in $J_1^{AA}(\omega_a) = 2W_n$ vs the $J_0^{AA}(0)$ obtained from T_2^{-1} is exactly the anomaly reported by GRF for PDT in S2 that they could not explain by the Moro–Nordio model of roto-translational coupling. Instead they suggested this observation could be fit by a SRLS model. Our successful fits to the 2D-ELDOR spectra using the SRLS model seem to confirm this. (Note that for the S_B and C phases this ratio increases further to 3–4.)

GRF were able to study the angular dependence of W_n for PDT in S2. Given that W_n is almost an order of magnitude smaller in the present case, we were limited to more qualitative observations. However, we observed substantial angular variation of the T_2^{-1} , whereas GRF found them to be only weakly orientation-dependent for PDT in S2. Thus it is difficult to compare the two results further. Instead, we compare the predictions for the spectral densities obtained with the SRLS and standard models using our fits to the $\Theta = 0^\circ$ spectra with the experimentally measured (and estimated) spectral densities for 57 °C shown in Fig. 5 and given in Table II. These simulations are shown in Fig. 10. We find that the angular variation of $J_0^{AA}(0, \Theta)$ and $J_0^{Ag}(0, \Theta)$ predicted by the SRLS model appear to be in reasonable agreement with the experimental observations, although the predicted magnitudes are somewhat larger, including a somewhat larger angular variation in $J_0^{AA}(0, \Theta)$. In a similar fashion we obtained predicted values of $2W_n$ vs Θ for 57 °C. These values show the substantial decrease in W_n for $\Theta \neq 0^\circ$, in accord with our qualitative observations. Here $2W_n$ is predicted to be somewhat smaller than observed at $\Theta = 0^\circ$ (cf. Table I). We note that the T_2^{-1} 's were estimated from the COSY measurements, which were obtained under different conditions, including slightly different temperatures, than the 2D-ELDOR experiments. This may be the explanation for at least part of the discrepancy in magnitudes (cf. below, where a related comparison is made utilizing only the 2D-ELDOR data). Given the very good simulations obtained in the global fits using the SRLS model in the S_A phase [see, e.g., Fig. 7(c)], any remaining discrepancy may be taken as an indication of some differences between the global fits to the full set of 2D-ELDOR data and the simplified analyses based on estimating T_2^{-1} 's from the COSY measurements and the LPSVD approach to obtaining W_n . As stated earlier, we clearly favor the global fits, which make full use of all the 2D-ELDOR spectra, and they do not ignore any incipient slow-motional effects (cf. the $R^c \geq 10^8 \text{ s}^{-1}$). These simulations do make clear that the SRLS model does lead to substantially enhanced values of the homogeneous linewidths without appreciably enhancing W_n , in accordance with the expectations of GRF.

Undoubtedly improvements can be made in the SRLS model that we have employed. There is sufficient evidence of roto-translational coupling from the anisotropic translational diffusion coefficients measured for PDT in S2 and from the considerations of GRF that one would like to modify the present SRLS model. In particular, we envision a

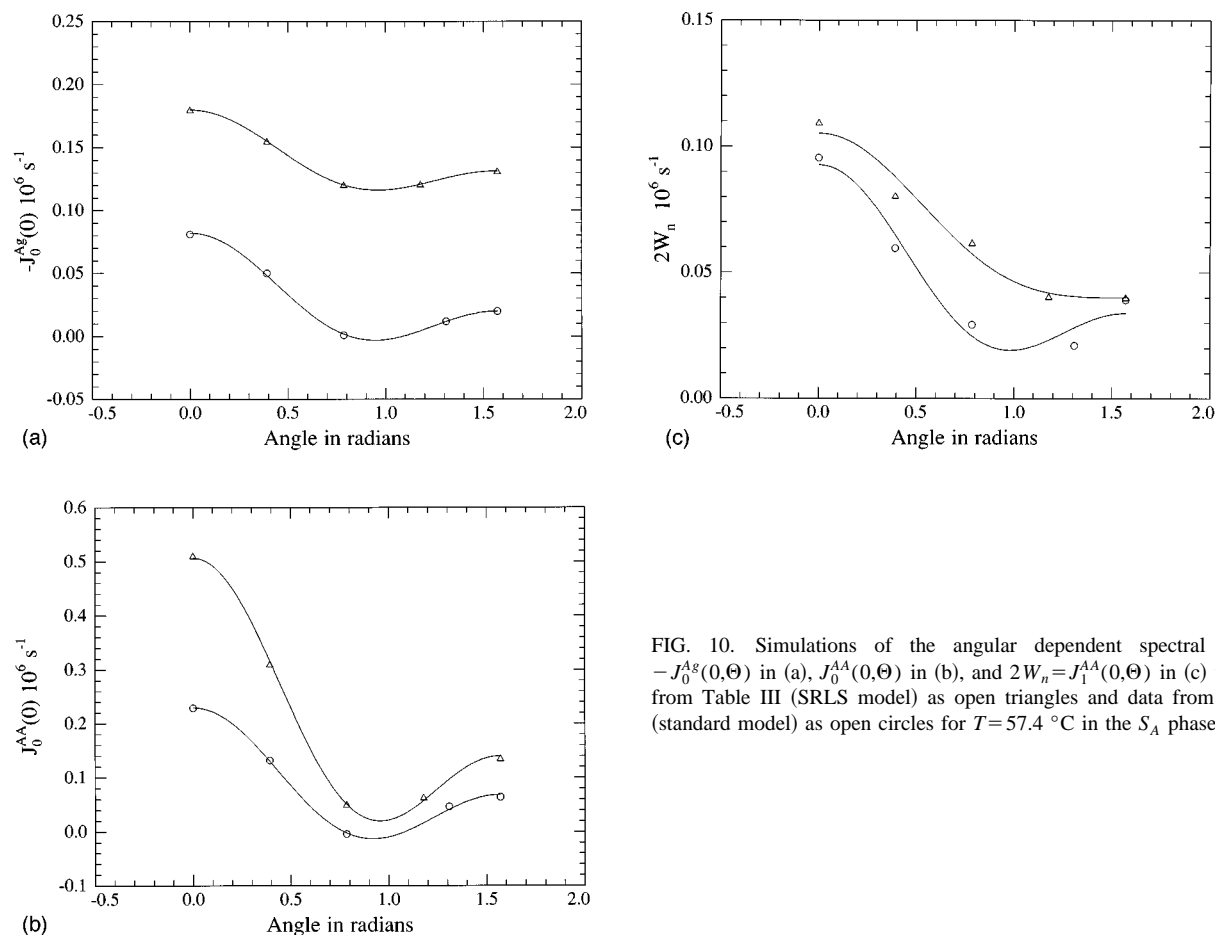


FIG. 10. Simulations of the angular dependent spectral densities: $-J_0^{Ag}(0, \Theta)$ in (a), $J_0^{AA}(0, \Theta)$ in (b), and $2W_n = J_1^{AA}(0, \Theta)$ in (c) using data from Table III (SRLS model) as open triangles and data from Table IV (standard model) as open circles for $T = 57.4^\circ \text{C}$ in the S_A phase.

modified SRLS model, wherein the nature of the cage (specified by c_0^2 , c_2^2 , and R^c) becomes a function of z , the location in the smectic layer. Thus, the diffusion of PDT through a smectic layer would lead to a variation in the cage seen by the PDT molecule. The disadvantage of such a model is, of course, the increased number of fitting parameters. This could only be justified in the context of even more independent experiments, such as including the 2D-ELDOR as a function of tilt angle Θ , and/or 2D-ELDOR experiments at a series of different frequencies (and magnetic fields). (A further modification to the model could be an anisotropic viscosity sensed by the local structure or cage, as proposed by LF.)

Finally, we wish to comment that there is no anomalous variation of the T_2 or W_n with mixing time as shown in Figs. 11 and 12, respectively. These data were obtained from the 2D-ELDOR spectra by using the LPSVD methods described in Sec. III for obtaining spectral densities. They show there is no significant very slow process such as director fluctuations in the time scale of the experiment corresponding to a maximum $T_m = 1.4 \mu\text{s}$. The T_2 's correspond to the S_A phase (57.4°C), and the W_n 's are shown for the S_A phase (57.4°C) and the I phase (89.8°C). Note that the spectral simulations were used to obtain W_n from the SRLS analysis at these two temperatures. They also show no variation in W_n with T_m consistent with experiment. That is, the cage has a τ_c of

$5.3 \times 10^{-9} \text{ s}$ at 89.8°C and $1.41 \times 10^{-9} \text{ s}$ at 57.4°C , which still corresponds to a fast time scale relative to T_m in our experiments. Note also that the simulated W_n values are in rather good agreement with the experimental results for the S_A case, but there are mild discrepancies for the I case. (Here the comparisons utilize the same 2D-ELDOR experiments

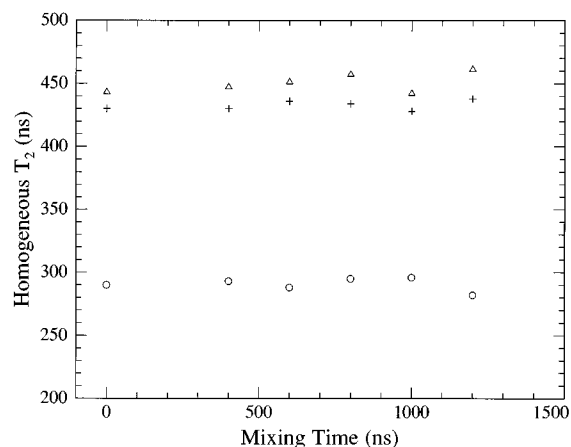


FIG. 11. Variation of homogeneous T_2 of different hyperfine lines with mixing time [$M_I = -1$ (plus signs); $M_I = 0$ (open triangles); $M_I = +1$ (open circles)]. From echo based analysis of the experimental ELDOR data at 57.4°C .

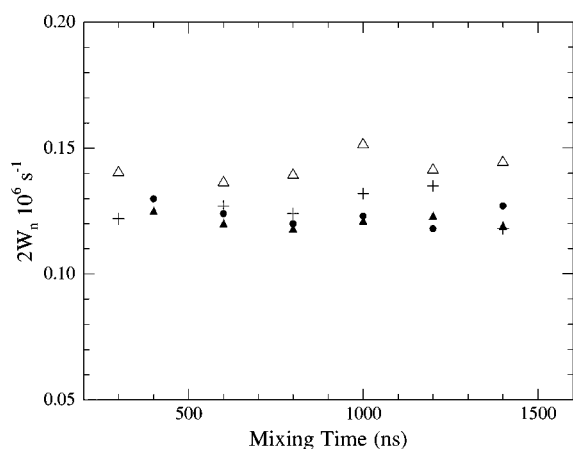


FIG. 12. Plot of $2W_n = J_1^{AA}(0)$ vs mixing time, T_m . The open triangles and pluses are for the isotropic phase (89.9 °C) and are experimental and simulated results, respectively. The filled triangles and filled circles are for the S_A phase (57.4 °C) and are experimental and simulated results, respectively. Simulations are for the SRLS model and use data from Table III.

unlike the comparison of fits from 2D-ELDOR to the COSY data discussed above.)

In the present study on PDT in 4O,8 we were not able to make significant use of the results obtained in the nematic phase because of its narrow temperature range and the large quasi-critical effects associated with the phase transitions. In the case of CSL in 4O,8 reported in Paper I, this did not appear to be a problem. That is, the normal spin relaxation of CSL yields very broad lines and large W_n 's. This is due to R_1^o of CSL being about 2 orders of magnitude smaller than that for PDT, and R^c for CSL at least an order of magnitude smaller than that for PDT but with $(S_{1,0}^2)^2$ several times greater. Thus the normal contributions for CSL can be much larger than the quasi-critical contributions, which are about the same as for PDT (except that they are amplified somewhat by the increase in $(S_0^2)^2$ for CSL vs PDT, an amount that is approximately offset by the $(S_{1,0}^2)^2$ factor in the SRLS contribution).⁵

V. CONCLUSIONS

The SRLS model of a dynamic cage has been successfully applied to the 2D-ELDOR spectra for the PDT probe in the isotropic and liquid crystalline phase of 4O,8. It leads to significantly improved fits compared to the standard model of Brownian reorientation in a macroscopic orienting potential. (The exception is the nematic phase, which has significant quasi-critical effects associated with the $N \rightarrow I$ and $N \rightarrow S$ phase transitions.) The cage structure persists through all the phases leading to a local ordering for PDT that is somewhat greater than its ordering in the macroscopic aligning potential of the ordered phases. The cage relaxes about two orders of magnitude slower than the probe, consistent with the physical assumptions of the SRLS model. The unusually rapid and nearly constant motional rate of the probe and dynamic cage parameters through all the phases was considered to be consistent with the model of gradual expul-

sion of PDT from the aromatic core region to the more labile aliphatic chain region as the temperature is lowered through the various phases. This is in marked contrast to the CSL probe, which shows a freezing out of the cage in the S_B and C phases. Overall, the use of global fitting by NLLS was found to be a more reliable and convenient method for obtaining optimum model parameters than the decomposition into the various spectral densities.

ACKNOWLEDGMENTS

This work was supported by National Science Foundation Grants Nos. DMR 9210638 and CHE93 13167 and NIH Grants Nos. GM25862 and RR07126. A.P. acknowledges the support of the Italian Ministry for Universities and Scientific and Technological Research and thanks Professor P. L. Nordio and Professor G. J. Moro for enlightening discussions. The computations reported here were performed at the Cornell Theory Center.

- ¹V.S.S. Sastry, A. Polimeno, R.H. Crepeau, and J.H. Freed, preceding paper, *J. Chem. Phys.* **105**, 5753 (1996).
- ²C.F. Polnaszek and J.H. Freed, *J. Phys. Chem.* **79**, 2283 (1975).
- ³W.J. Lin and J.H. Freed, *J. Phys. Chem.* **83**, 379 (1979).
- ⁴J. Gorcester, S.B. Rananavare, and J.H. Freed, *J. Chem. Phys.* **90**, 5764 (1989).
- ⁵A. Nayeem, S.B. Rananavare, V.S.S. Sastry, and J.H. Freed, *J. Chem. Phys.* **96**, 3912 (1992).
- ⁶J.H. Freed, A. Nayeem, and S.B. Rananavare, in *The Molecular Dynamics of Liquid Crystals*, edited by G.R. Luckhurst and C.P. Veracini (Kluwer, Dordrecht, 1994), Chap. 12.
- ⁷J.K. Moscicki, Y.K. Shin, and J.H. Freed, *J. Chem. Phys.* **99**, 634 (1993).
- ⁸C.W. Garland, M. Meichle, B.M. Ocko, A.R. Kortan, C.R. Safinya, L.J. Yu, J.D. Litster, and R.J. Birgeneau, *Phys. Rev. A* **27**, 3234 (1983).
- ⁹F. Volino and A.J. Dianoux, *Mol. Phys.* **36**, 389 (1978).
- ¹⁰G. Moro, P.L. Nordio, and U. Segre, *Chem. Phys. Lett.* **105**, 440 (1984).
- ¹¹G. Moro, U. Segre, and P.L. Nordio, in *Nuclear Magnetic Resonance of Liquid Crystals*, edited by J.W. Emsley, NATO ASI Ser. C 141 (Reidel, Dordrecht, 1985).
- ¹²J. Gorcester, G.L. Milhauser, and J.H. Freed, in *Modern Pulsed and Continuous Wave Electron Spin Resonance*, edited by L. Kevan and M.K. Bowman (Wiley, New York, 1990).
- ¹³J. Gorcester and J.H. Freed, *J. Chem. Phys.* **85**, 5375 (1986); **88**, 4678 (1988).
- ¹⁴S. Lee, B. Patyal, and J.H. Freed, *J. Chem. Phys.* **98**, 3665 (1993).
- ¹⁵R.H. Crepeau, S. Saxena, S. Lee, B.R. Patyal, and J.H. Freed, *Biophys. J.* **66**, 1489 (1994).
- ¹⁶A. Polimeno, and J.H. Freed, *J. Phys. Chem.* **99**, 10995 (1995).
- ¹⁷S. Lee, D.E. Budil, and J.H. Freed, *J. Chem. Phys.* **101**, 5529 (1994).
- ¹⁸D. Budil, S. Lee, S. Saxena, and J.H. Freed, *J. Magn. Res. A* **120**, 155 (1996).
- ¹⁹D. Gamliel and J.H. Freed, *J. Magn. Reson.* **89**, 60 (1990).
- ²⁰J.S. Hwang, R.P. Mason, L.P. Hwang, and J.H. Freed *J. Phys. Chem.* **79**, 489 (1975).
- ²¹A. Nayeem and J.H. Freed, *J. Phys. Chem.* **93**, 6539 (1989).
- ²²R.R. Ernst, G. Bodenhausen, and A. Wokaun, *Principles of Nuclear Magnetic Resonance in One and Two Dimensions* (Oxford University Press, New York, 1987).
- ²³W.H. Press, B.P. Flannery, S.A. Teukolsky, and W.T. Vetterling, *Numerical Recipes* (Cambridge University Press, Cambridge, 1986).
- ²⁴J.H. Freed, A. Nayeem, and S.B. Rananavare, in *The Molecular Dynamics of Liquid Crystals*, edited by G.R. Luckhurst and C.P. Veracini (Kluwer, Dordrecht, 1994), Chap. 14.
- ²⁵K.A. Earle, D.E. Budil, and J.H. Freed, *J. Phys. Chem.* **97**, 13289 (1993).
- ²⁶In the case of substantial non-secular contributions, the perturbation theory of GRF shows that the 2D-ELDOR cross-peaks could decay with T_m by additional exponentials. If such were the case, then our present analysis would lead to apparent W_n 's that vary as a function of mixing time, contrary to our results (cf. Fig. 12).